Final Report for the Office of Hydrologic Development
NATIONAL OCEANIC AND ATMOSPHERIC ADMINISTRATION
NATIONAL WEATHER SERVICE

Project title:

Towards Probabilistic Quantitative Precipitation WSR-88D Algorithms: Data Analysis and Development of Ensemble Model Generator: Phase 4

NOAA Contract:
DG133W-02-CN-0089

Principal Investigators:

Witold F. Krajewski and Grzegorz J. Ciach
IIHR-Hydroscience & Engineering
The University of Iowa
Iowa City, Iowa 52242

Report Authors:

Witold F. Krajewski, Grzegorz J. Ciach, and Gabriele Villarini
IIHR-Hydroscience & Engineering, The University of Iowa

June 2005

EXECUTIVE SUMMARY

The report describes progress made towards developing a scientifically rigorous methodology for operational probabilistic quantitative precipitation estimation (PQPE) for hydrologic applications. The methodology will be based on the WSR-88D measurements complemented with rain gauge and satellite data. It is flexible enough to allow a smooth transition to the polarimetric era after the planned upgrade of the operational network of radars. The overall strategy is to demonstrate hydrologic utility of the probabilistic information of the precipitation estimates. This involves two major elements (1) developing a theoretical and operational framework for probabilistic radar-rainfall estimation; and (2) connecting the PQPE input with a hydrologic application. This report documents initial progress made in both elements.

The authors define a radar PQPE product as a set of situation-dependent parameter values in a model describing the probability distributions of the uncertainties in the radar-estimated rainfall. The distributions quantify the available probabilistic knowledge about the true spatial rainfall that is likely, given current radar measurements and other available information. The model parameter values determine unambiguously the uncertainty distributions for each operationally useful distance from the radar and spatiotemporal averaging scale. This allows generating different user-specific outputs demanded by various operational applications. Among these outputs are the uncertainty bounds and probabilities of exceedence. Generating an ensemble of the probable rainfall maps to provide the input for the ensemble forecasting schemes is also possible. The report presents early results of the model formulation.

The hydrologic utility of the PQPE methodology will be demonstrated using the flash flood forecasting problem. This part of the project is performed in close collaboration with the Hydrologic Research Center (HRC). The demonstration is limited geographically to the Oklahoma region. This report documents developments leading to PQPE application in a Flash Flood Guidance and Monitoring system. The authors present uncertainty analysis of the Thresh-R model which is the basis for FFGM and of the soil moisture accounting model. The early results also include effect of the uncertainty in the rainfall input via an example of ensemble PQPE simulation.

Useful Acronyms

ABRFC	Arkansas Basin River Forecast Center
CDP	conditional distribution of precipitation
CSI	Critical Success Index
DHR	Digital Hybrid Scan Reflectivity
DPA	Digital Precipitation Array
FAR	False Alarm Ratio
FFG	Flash Flood Guidance
FFMP	Flash Flood Monitoring and Prediction
HL	Hydrologic Laboratory
HRC	Hydrologic Research Center
HRAP	Hydrologic Rainfall Analysis Project
KDP	specific differential phase shift
KINX	WSR-88D in Tulsa, OK
KTLX	WSR-88D in Twin Lakes, OK
MAP	Mean Area Precipitation
MFB	Mean-field-bias
MPE	Multisensor Precipitation Estimation
NCDC	National Climatic Data Center
NSSL	National Severe Storms Laboratory
NWS	National Weather Service
PED	product-error-driven
POD	Probability of Detection
PPS	Precipitation Processing System
PQPE	Probabilistic Quantitative Precipitation Estimation
RFC	River Forecast Center
SOW	Statement of Work
WFO	Weather Forecast Office
WSR-88D	Weather Surveillance Radar - Doppler
Z	radar reflectivity
ZDR	differential reflectivity
CSSA	Convective/Stratiform Separation Algorithm
REC	Radar Echo Classifier
RCA	Range Correction Algorithm
EPPS	Enhanced PPS
HCA	Hydrometeor Classification Algorithm
EPRE	Enhanced Preprocessing

TABLE OF CONTENTS

A. BACKGROUND INFORMATION

Hydrologic forecasting and water resources services performed for the public by the National Weather Service (NWS) require decision making in presence of uncertainty due to limitation in our understanding of nature, available information, and predictability of natural phenomena. High space and time resolution precipitation estimates are the main input for many of the forecasting and decision support models and systems. These estimates are based on information from the network of weather radars WSR-88D combined with rain gauge and satellite data (e.g. Fread et al. 1995; Stallings and Wenzel 1995). The current operational NWS multi-sensor rainfall algorithms produce only deterministic fields of precipitation intensity and accumulations (e.g. Fulton et al. 1998). The operationally provided rainfall products are deterministic in the sense the sense that, while significant error associated with these products are widely acknowledged, no quantitative information on their magnitude associated with the products is routinely available. Users of these products would be better able to make informed decisions if they knew not only the best rainfall estimate but also the associated uncertainty and/or range that most likely includes the actual amount of rainfall that occurred.

The Office of Hydrologic Development of the NWS intends to address this shortcoming of the existing algorithms by preparing a comprehensive plan for development of a new generation of algorithms for the precipitation estimation. These algorithms are referred to as *probabilistic quantitative precipitation estimation*, or PQPE. Krajewski and Ciach (2003) developed a comprehensive plan for nation-wide development of the PQPE algorithms. Their report lays out an early formulation of the problem, identifies conceptual, methodological and technological issues, and proposes a feasible plan of action. However, because the plan calls for considerable expenditures of resources, the PQPE Advisory Team suggested preceding it with a geographically focused effort of an end-to-end demonstration of the utility of the PQPE approach. In response, Krajewski et al. (2003) formulated a plan for developing such a demonstration.

In this report we present first results of an extensive data analysis and development of an initial version of ensemble generator that could be used operationally to provide users with plausible realizations of rainfall fields. Following Krajewski et al. (2003), we describe (1) a formulation of the radar-only PQPE algorithm; (2) the corresponding extensive data analyses and identification of appropriate model and estimation of its parameters based on actual data from Oklahoma; and (3) the ensemble generator and examples of its workings with potential operational use.

B. FORMULATION OF THE PQPE METHODOLOGY

During the Phase II of this project, we continued our analysis and refinement of the methodological framework for the PQPE problem that was initiated in Phase I (Krajewski and Ciach 2003). For the completeness of this report, we briefly summarize the proposed methodology for the PQPE algorithm development as we understand it now.

B.1. Basic Definitions

The four fundamental notions defined below are used throughout this report:

- *True rainfall*: The amount of rain-water that has fallen on a specified area in a specified time-interval.
- *Radar-rainfall (RR)*: An approximation of the true rainfall based on radar data corresponding to the same spatio-temporal domain.
- *RR uncertainties*: All systematic and random differences between RR and the corresponding true rainfall.
- *Ground reference (GR)*: Estimates of the area-averaged rainfall accumulations based on rain-gauge data that are used to evaluate RR products.

B.2. Problem Description

The progressive evolution of the operational RR products has been guided by the attempts to quantify and to reduce the uncertainties in the RR estimates. The currently existing RR maps produced operationally by the NWS (the Stage II and III products) are just arrays of numbers describing the spatial distribution of approximate rainfall accumulation values that are obtained based on the WSR-88D reflectivity measurements corrected with the available concurrent rain-gauge data. Application of the term "quantitative precipitation estimates" QPE to such products implies that the maps are completed with quantitative information about the product uncertainties. Without such information about the relation of the RR product to the corresponding true rainfall, both the notion of "quantitative" and the mathematical term "estimation" would be meaningless in this context. However, despite a wide use of this term, the operational QPE products are devoid of their uncertainty information. We believe that the development of the probabilistic quantitative precipitation estimation (PQPE) products based on sound empirical evidence will be the optimal comprehensive solution for this pathological situation.

The probabilistic products, both in meteorology and hydrology, convey the inferred information about the unknown true value of a physical quantity in terms of its probability distribution rather than its one "best" estimate (e.g. Krzysztofowicz 2001). Thus, the radar PQPE product can be mathematically defined through the conditional probability distributions of the likely true rainfall, given the current radar measurements and other available information. These distributions can be determined by specific parameter values of a general uncertainty

distribution model developed in this project. The model parameters have to determine unambiguously the uncertainty distributions of given RR estimates in different rainfall regimes for each operationally useful distance from the radar and spatio-temporal averaging scale. From such a general PQPE product, one can directly derive any specific uncertainty characteristics (for example, the RR expectation, standard errors, probabilities of exceedence, or an ensemble of probable rainfall maps) that can be required for different operational applications.

B.3. Basic Requirements

During the discussions with the panel of experts engaged in the Phase I of this project (Krajewski and Ciach 2003), it was agreed that any method that will be applied to generate the PQPE products has to satisfy several key requirements. These requirements were further analyzed and refined in the course of the Phase II of the project. We summarize them briefly below:

1. The method has to be empirically "verifiable." Conditions have to be assured to systematically evaluate the degree of agreement between the PQPE results and the RR uncertainties estimated based on reliable GR in selected "validation sites."

2. The method has to be adjustable to different synoptic and topographical situations, and to the changing operational environment, by its model parameter calibration using available information.

3. The method has to account for the spatio-temporal dependencies in the errors process to provide the PQPE products over a broad range of spatial and temporal scales used in different hydrological applications.

4. The method has to work with the current reflectivity-only WSR-88D algorithms, the multi-parameter (MPE) algorithms using the available concurrent rain-gauge and satellite data, and the polarimetric algorithms (using differential reflectivity and differential phase-shift) available operationally after the upcoming upgrades of the WSR-88D radars.

5. The method has to provide the PQPE products in a format appropriate for their efficient usage in different hydrological applications.

B.4. Development of the PQPE Algorithm

During the previous phases of this project, it has been agreed that the product-error-driven (PED) modeling approach for the PQPE algorithm, described in our reports for the Phase1 and Phase 2, will be developed using a fully empirically-based framework. This decision acknowledges the obvious fact that building a PQPE algorithm has to be preceded by the development of a realistic and parsimonious mathematical model of RR uncertainties underlying the probabilistic nature of RR products. Only a thorough and comprehensive data analysis can result in the identification of such a realistic model suitable for the PQPE applications.

However, the actual exploratory data analysis of the PPS products has not started yet because the preparation of the data sample has not been completed. Therefore, the algorithm development efforts in the Phase 3 concentrated on the following tasks:

1. Development of the PED modeling methodology;
2. Preparation of the large data sample;
3. Testing the GR error filtering method.

Below, we briefly describe the work performed in these tasks and the results that have been achieved so far.

B.4.1. Development of the PED Modeling Methodology

There are many sources of errors in RR products and we discussed them in the Phase 1 report. The PED approach focuses on the combined effect of all the errors, its modeling, and estimation of the model parameters. This follows the fact that one cannot delineate the separate effects using the available measurable quantities. In practice, only the combined effect on the RR estimates can be measured and quantified. Our objective is to create a flexible parameterized mathematical model of the relation between the RR product values and the corresponding True Rainfall conditioned on different situations. The four conditions that we plan to quantify are the distance from the radar, space-time averaging scale, rainfall regime, and the PPS setup. In the PQPE algorithm, this model will be used to quantify the probability distributions of the probable True Rainfall, given the RR value and the other abovementioned conditions.

B.4.1.1. *General Structure of the Model*

The relationships between RR and the corresponding truth can be described by the family of the conditional bivariate frequency distributions that we call the "true verification distributions" (TVD):

$$(R_a , R_r)_{L,T,d,S} = f(R_a , R_r \mid L, T, d, S) \quad (1)$$

where R_a and R_r are the corresponding (concurrent and collocated) True Rainfall and RR values, respectively, L is the spatial averaging scale, T is the temporal scale (accumulation interval), d is the distance from the radar station, and S denotes the type of the precipitation system (rain regime). In principle, these distributions can be retrieved from the radar-gauge data samples, if additional information on the rainfall variability is available (see section B.4.3 below).

To simplify the notation, we can focus on one spatiotemporal resolution (L, T), distance (d) from the radar and rain regime (S). To model the (R_a , R_r) distribution for these specified conditions, it is convenient to use the following functional-statistical representation:

$$R_a = h(R_r)\, e(R_r) \quad (2)$$

where $h(\cdot)$ is a deterministic distortion function, and e is a random variable representing the random uncertainties that we call the multiplicative random uncertainty factor. If parametric models of the deterministic function, $h(R_r)$, and the stochastic function, $e(R_r)$, are identified and its parameter estimates conditioned on a specific situation are known, this representation prescribes the way in which the ensembles of probable True Rainfall values, or only its selected statistical characteristics required by the users, can be generated for each given value of RR.

B.4.1.2. *Main Elements of the Model*

Because all systematic biases can be described by the deterministic distortion function, we can assume without any loss of generality that the mean of the random uncertainty factor is always equal to unity ($E\{e\}=1$). This allows the rigorous definition of the $h()$ function based on the general regression formula:

$$h(x) = E\{R_a \mid R_r=x\}, \tag{3}$$

which, in practice, can be identified and estimated using any version of the nonparametric regression apparatus (Hardle 1990; Simonof 1996).

Although the mean of the multiplicative random uncertainty factor, $E\{e(R_r)\}$, is equal to unity for each value of R_r, its distribution can vary with R_r. The first step in identifying this dependence is to estimate the $e(R_r)$ variance as a function of R_r. This can be done in the similar way as estimating the $h(R_r)$ function. An example of such a procedure is shown in the section B.4.1.3 below. Next, we have to find a suitable parametric model for the $e(R_r)$ distributions. This can be achieved based on extensive data analysis by examining the shapes of the actual $e(R_r)$ distributions under different values of the conditioning factors. Since the extreme rainfall events are the most important in hydrological practice, it is essential that the selected probability distribution model describes the uncertainty distribution tails with a reasonable accuracy. Examples of the models that have distinctly different tails are the gamma, lognormal and beta distributions. Each of them can lead to different decisions based on the PQPE results. The goodness-of-fit of these and several other models will have to be tested on the large data sample before a justified choice can be made.

Once parametric models of the $h(R_r)$ function and the $e(R_r)$ variable (or the family of random variables indexed by R_r) are identified, the dependence of their parameters on the averaging scale (L, T), distance from the radar (d) and rain regime (S) can be estimated based on the family of the verification distributions (estimated bivariate distributions of RR and the corresponding True Rainfall):

$$(R_r\ ,\ R_a)_{Ln,Tn,d,S}\ ,\ \ n=1,\ 2,\ \ldots\ ,\ N_{max} \tag{4}$$

where the distributions are sampled for several spatio-temporal scales that are multiples of the original RR product scale. Spatio-temporal dependencies in the model parameters can then be modeled to reproduce the dependence of these conditional model parameter estimates on the discrete series of scales (A_n ,T_n), for each given distance from the radar (d) and precipitation regime (S).

It is still unclear to us how to stratify the data sample according to the precipitation regime (S) so that this information is meaningful for the PQPE methodology. The appropriate classification has to be based on data that are readily operationally available during the PPS processing, preferably the radar data. In addition, it should exhibit distinct differences in the PED model parameter values for the different regimes. One of such classification schemes by Steiner et al. (1995) has been investigated by Ciach et al. (1997). Our results indicated that its effects on the RR estimation algorithm are practically the same as the stratification of the data sample according to different RR values. Consequently, using this specific precipitation regime classification can only complicate the PQPE algorithm unnecessarily without adding any value to it. A classification of the synoptic situation, or some other information (e.g., the zero isotherm level) based on the operational weather forecasts could perhaps be a better alternative to the schemes using the radar data only. However, the best way to use this external information remains to be investigated. We hope that the PQPE Advisory Team will help us with this issue.

Obviously, the successful development of operationally applicable parametric models of the $h(R_r)$ function and the $e(R_r)$ variable will most likely require a number of generalizations and simplifications in the mathematical description of the abovementioned dependences. The specific formulas will have to be identified during the planned extensive analysis of large data samples.

B.4.1.3. *Preliminary Analysis of RR Error Structure*

In the Phase 3 of this project, we performed a preliminary study of the basic elements of the RR error structure. It is an extension of our first analysis that we described in the Phase 1 report. This analysis is based on a relatively small data sample of 50 rainy days and its main purpose was to develop and test the first version of the data processing and functional estimation tools that will be applied to the large samples of the operational RR products. The radar data from the Tulsa, Oklahoma, NEXRAD station (KINX) were quality controlled and converted into hourly accumulations in polar grids over 23 surrounding rain gauge stations (Vignal and Krajewski 2001).

Because there are two variables the (R_a , R_r) distribution, there exist two mathematically equivalent ways to represent it in the form of a functional-statistical relationship between these variables. The first of them is defined in Equation (2), whereas the second is obtained by exchanging the R_a and R_r variables in this Equation. Although the second representation is more suitable for characterizing the RR error structure that for building the PQPE ensemble generator, we used it in this preliminary analysis to obtain results that are formally comparable with the results that we had obtained previously. From the point of view of the estimation technique, both representations are exactly the same and the same data processing tools can be applied to both of them. However, to avoid confusion, we denote the equivalent deterministic and random components as h_1 and e_1, respectively. Additionally, we simplified the analysis by assuming the raingauge rainfall accumulations, R_g, for the approximations of the true rainfall R_a. In fact, using our area-point error filtering procedure (see section B.4.2) was impossible for this sample due to the lack of the corresponding small-scale rainfall variability data.

Using the 50-storm data sample, we estimated the deterministic error function, $h_1(\cdot)$, and the variance of the multiplicative random error, $e_1(\cdot)$, as functions of the accumulation time. At this stage, we did not consider the dependences on the spatial scale, distance from the radar, or the rain regime. The temporal dependences in the RR error process were estimated for five

accumulation intervals: 1, 3, 6, 12, and 24 hours. The deterministic distortion function was estimated using the following scheme of moving-window averaging:

$$h_1(r) \approx < R_r \mid r\text{-}u \le R_g \le r+u > \qquad (5)$$

where R_g is the rain gauge rainfall accumulation and u is the averaging window size. The window size was increased with R_g to compensate for the decreasing number of data points. These functions, for the five time scales, are shown in Figure 1.

The results in Figure 1 show that the systematic distortion component is a nonlinear function of the True Rainfall. This function is a way to quantify the conditional biases in different RR products that have been qualitatively demonstrated long time ago by Austin (1987) and investigated using an idealized analytical model by Ciach et al. (2000). For the larger accumulation intervals (6, 12 and 24 hours), these conditional biases are relatively small and invariant in respect to the time-scale. The outstanding results for the 1-hour and 3-hour time-scales might be the effect of large rain gauge representativeness errors, however, they might as well indicate a distinctly different uncertainty structure at the short scales. This question requires more extensive analyses using the area-point error filtering method described in section A.1.3 below.

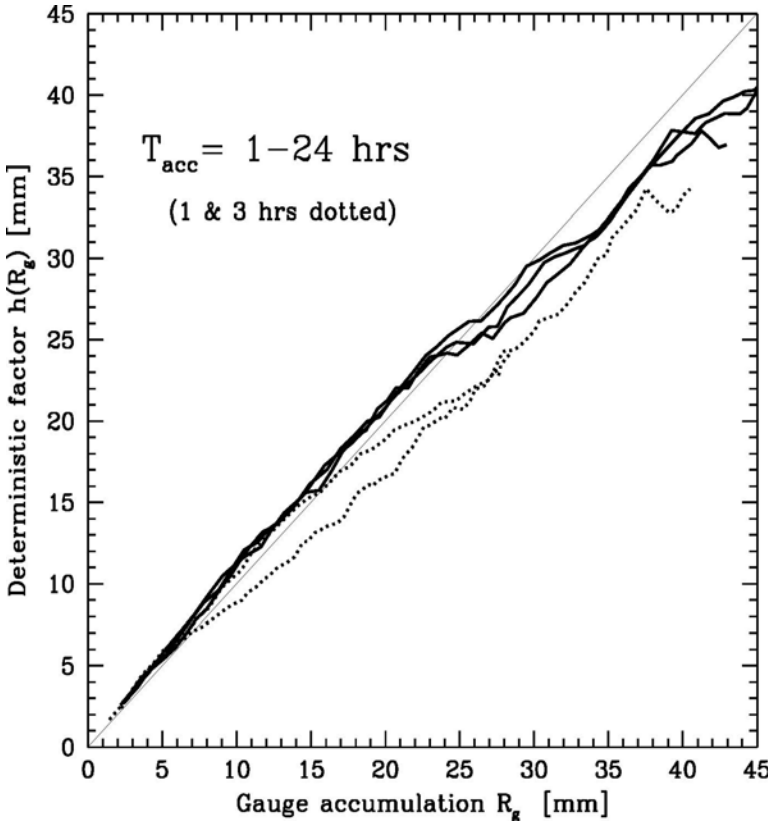

Fig. 1. Systematic distortions, h, as functions of True Rainfall for the five accumulation intervals.

The standard deviation of the random error factor as a function of the rain gauge rainfall accumulation for the same five accumulation intervals is shown in Figure 2. The $e_1(\cdot)$ variances, σ_{e1}^2, as a function of R_g were estimated in a similar way as the $h_1(\cdot)$ functions:

$$\sigma_{e1}^2(r) \approx < (e_1(R_g)-1)^2 \mid r-u \le R_g \le r+u > \qquad (6)$$

using the same moving-averaging scheme with variable window size.

The results in Figure 2 show that, for each of the five accumulation intervals, the standard deviation of the multiplicative random uncertainty factor decreases rapidly with increasing rainfall and then stabilizes at the level of about 30%. The estimates of the random component seem to be less sensitive to the shorter time-scales than the estimates of the systematic distortion function. This invariance, if confirmed on the large data sample that we currently prepare, can be a good basis to reduce the number of parameters of the final PED model that will be used for the PQPE algorithm.

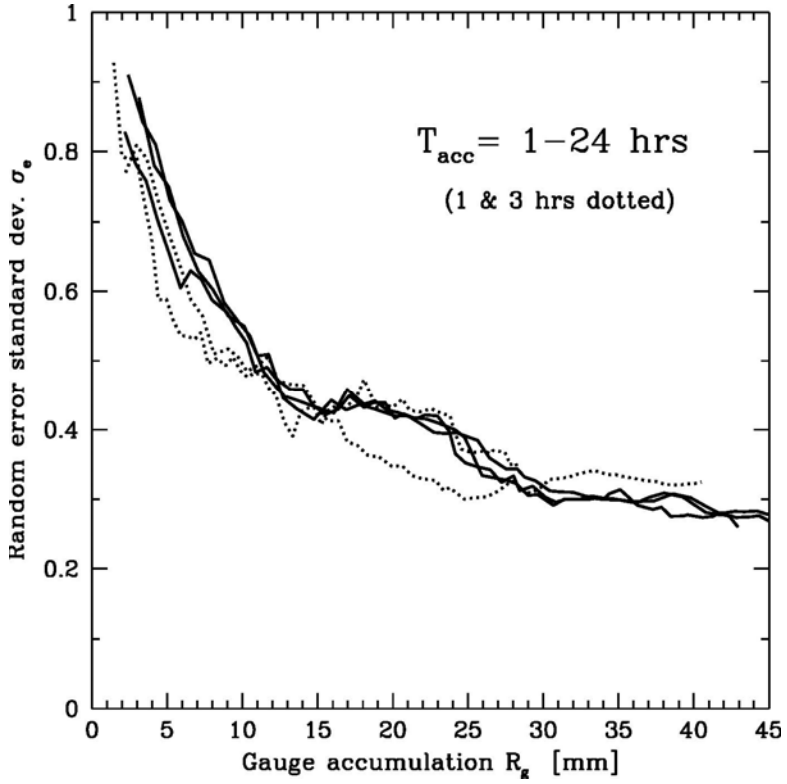

Fig. 2. Standard deviations of the multiplicative random error factor, *e*, as functions of True Rainfall for the five accumulation intervals.

Note that the results shown in Figures 1 and 2 are based on a research sample that was carefully selected and quality controlled. A well tested and sample-calibrated ground clutter and

AP reduction procedure based on a neural-network algorithm was applied prior to the Z-R conversion (Vignal and Krajewski 2001). The coordinate transformation errors are not present because the RR estimates are only in the polar coordinates. Additionally, a correction of the vertical profile of reflectivity (VPR) reduced the RR errors considerably at larger distances (Vignal and Krajewski 2001). Consequently, the uncertainties presented above can be significantly smaller than what we would obtain based on the operational PPS products. Therefore, it is essential to repeat the analysis on the large sample of the PPS products that we described in section C.1.

B.4.1.4. *Two Idealized Implementations*

One of the most difficult elements of the PQPE methodology concerns including the spatial and temporal dependences that exist in the RR uncertainty process into the probabilistic model that we create using the PED approach. In the course of developing a viable technique to treat this problem, we started with two idealized implementations of the PQPE algorithm that are based the following simple model of the (R_a , R_r) distribution:

$$R_a = R_r \, e \tag{7}$$

where the random uncertainty factor, e, is lognormally distributed and does not depend on the RR value (a multiplicative homoscedastic model). Both algorithms are designed to simulate ensembles of the probable true rainfall conditioned on the RR values obtained from the radar data. The first algorithm includes the temporal dependences in the uncertainty process, whereas the second algorithm generates ensembles of spatially correlated uncertainty fields. These dependences in the e variable were modeled based on a meta-Gaussian model that starts with a time series (or spatial field) of the uncorrelated standard normal white noise. Next, this variable is correlated in time (or space) using weighted moving-window averaging with a specified averaging mask, and the outcomes are transformed into the positively defined random process through the exponential transformation. The parameters of this transformation are such that the resulting variable has the mean equal to unity and the specified variance.

The temporally correlated 1-D version of this simple PQPE algorithm was applied to generate the ensembles of time-series of probable true rainfall for the lumped flash flood forecasting model that we implemented and upgraded into probabilistic framework with the help of the Hydrologic Research Center. This numerical experiment is a part of the PQPE project and is described in section A.2 of this report. The flow-chart of this algorithm consists of the following steps:

1. Generate an 1-D array of independent standard normal deviates.
2. Apply the weighted moving-window averaging to the array.
3. Apply the exponential transformation to the smoothed array.

This procedure generates one time-series of the time-correlated meta-Gaussian uncertainty process. It is repeated to obtain the required number of the ensemble members. The weighted moving-window averaging can, in principle, be performed using any averaging mask. This

allows fairly flexible adjustment of the simulated temporal uncertainty structure to the empirical estimates that we will obtain from the data analysis. At this stage, we used a simple polynomial mask for this smoothing. The parameters controlling the algorithm outcomes are:

1. The number of realizations in the ensemble.
2. The length of the simulated time-series.
3. The size and shape of the smoothing mask.
4. The standard deviation of the uncertainty factor.

The 1-D algorithm described above is fast and enables generating large ensembles consisting of 10^5, or more, realizations for the probabilistic hydrological forecasting model. However, it can only be applied to the lumped rainfall-runoff models.

The spatially correlated 2-D version of the PQPE algorithm was applied to generate the ensembles of spatial fields of probable true rainfall. It can be applied to a distributed hydrological forecasting model, or used to compute the RR uncertainty bounds for different spatial scales. The flow-chart of this algorithm consists of the following steps:

1. Generate a 2-D array of independent standard normal deviates.
2. Apply the weighted moving-window averaging to the array.
3. Apply the exponential transformation to the smoothed array.

This procedure simulates one field of the space-correlated meta-Gaussian uncertainty process and is repeated to generate the required number of the ensemble members. The weighted moving-window averaging can, in principle, be performed using any averaging mask. It can also be adjusted to the empirical estimates that we plan to obtain from the data analysis. The parameters controlling the algorithm outcomes are:

4. The number of realizations in the ensemble.
5. The size of the simulated spatial array.
6. The size and shape of the smoothing mask.
7. The standard deviation of the uncertainty factor.

The 2-D algorithm described above is computationally demanding and the largest ensembles that we generated so far consisted of up to 10^3 realizations. However, it can be used in a much broader range of applications than the 1-D algorithm. Therefore, it will be the basis for the development of the full PQPE algorithm. During its further development, we will extend the simulation procedure to include the dependences of the uncertainty factor on the RR values and the distance from the radar, and implement different probability distribution models.

B.4.2. GR Error Filtering

We developed a conditional distribution transformation (CDT) method for improving RR uncertainty analyses that use sparse rain gauge networks as the ground reference. The objective of the CDT method is perform a conditional point-area rainfall distribution transformation in order to filter out the rain gauge representativeness errors from radar-rain gauge samples. The

application of the rain gauge error filtering is essential for the estimation of the spatial dependences in the PQPE model because large differences between the sampling areas of radar and rain gauge measurements can render the results of direct comparisons meaningless. We tested the validity and evaluated the accuracy of the CDT method. The tests were based on the data from the USDA Agricultural Research Service Micronet. A detailed description of the CDT method and its tests has been documented in Habib at al. (2004). Below, we present only an outline of this effort and its results.

B.4.2.1. *Point-Area Distribution Transformation Method*

Our implementation of the point-area transformation scheme follows in principle the methodology presented in Morrissey (1991). Let R_p represent point (single rain gauge) rainfall with mean $E\{R_p\}$ and variance $Var\{R_p\}$, and R_a represent the rainfall averaged over an area A with mean $E\{R_a\}$ and variance $Var\{R_a\}$. The means of the two corresponding processes are equal, i.e. $E\{R_a\}=E\{R_p\}$, and the variances can be related to each other based on the spatial correlation in the rainfall field in the following way:

$$Var\{R_a\} = \frac{Var\{R_p\}}{A^2} \int_A \int_A \rho(x,y)dx^2 dy^2 \tag{8}$$

Now, given the probability distribution of R_p, we want to estimate the distribution of R_a that has the same mean as R_p, but different and known variance. As an approximate solution for this problem, we adopted a nonparametric distribution transformation method proposed by Journel and Huijbregts (1978).

The probability distribution of rain gauge measurements R_p can always be represented using a transformation that expresses R_p as a function of the standard normal random variable $R_p=\phi_{Rp}(u)$, where u is the standard Gaussian variable and the equality is in the sense of the same probability distributions (Journel and Huijbregts 1978). This function is approximated using a decomposition (expansion) based on Hermite polynomials:

$$\phi_{R_p}(u) \approx \sum_{i=0}^{n} \frac{\psi_i}{i!} H_i(u), \tag{9}$$

where $H_i(\cdot)$ are Hermite polynomials of the order i and ψ_i are their expansion coefficients, and the first four Hermite polynomials are shown as an example. The decomposition coefficients are fitted to the empirical frequency distribution of R_p using an iterative procedure described in Journel and Huijbregts (1978). The coefficients ψ_i are related to the mean and variance of the point rainfall as follows:

$$\psi_o = E\{R_p\}, \tag{10}$$

$$\sum_{i=1}^{n} \frac{\psi_i^2}{i!} = Var\{R_p\}. \tag{11}$$

The main assumption of the point-area transformation scheme proposed by Journel and Huijbregts (1978) is that the function ϕ_{Ra}, expressing the areal rainfall as a function of the standard normal random variable (just as ϕ_{Rp} represents the point rainfall), has the same Hermite expansion as ϕ_{Rp}, but its decomposition coefficients are modified by a single scaling factor, a, in the following way:

$$\phi_{R_a}(u) \approx \sum_{i=0}^{n} \frac{\psi_i a^i}{i!} H_i(u), \tag{12}$$

where the coefficients ψ_i are the same as in the point rainfall decomposition. Note that this distribution transformation preserves the distribution mean since $a^0=1$. On the other hand, the variance of the transformed distribution of the areal rainfall can now be expressed as:

$$Var\{R_a\} = \sum_{i=1}^{n} \frac{\psi_i^2 a^{2i}}{i!}, \tag{13}$$

and thus, it depends on the known decomposition coefficients ψ_i of the rain gauge rainfall and the scaling factor, a, only. This equation is a monotone function of a. Thus, if the variance of R_a is known, the scaling factor can be determined, using any iterative or graphical method, so that this equality is fulfilled.

Given the estimates of the coefficients, ψ_i, and the scaling factor, a, the computer generated standard normal deviates can be substituted into the Hermite expansion to simulate the distribution of the area-averaged rainfall. This point-area transformation procedure is general. It can be applied to the whole data sample, as well as to its sub-samples selected (conditioned) in any specific way. Since our focus in this study is on quantification of RR uncertainties, the distributions and their transformation have to be conditioned on the radar estimates, R_r.

The scheme of this conditional distribution transformation (CDT) can be summarized as follows. First, the rain gauge rainfall values in the data sample are grouped into sub-samples that are conditioned on a number of ranges of the RR values, ($R_p|R_r=r$), each range centered on a RR value, r. The number of the sub-samples and their sizes depend on the amount of available data. Then, the correlation function of the point rainfall conditioned on the radar estimate value, ($\rho|R_r=r$), is estimated. This enables the estimation of the conditional variances of areal rainfall, $Var\{R_a|R_r=r\}$. For each of the sub-samples ($R_p|R_r=r$), the conditional coefficients, ($\psi_i|R_r=r$), of the Hermite polynomial decomposition and the conditional scaling factors, ($a|R_r=r$), are estimated. Finally, the conditional distribution transformation functions ($\phi_{Ra}|R_r=r$) are computed

and used to generate values that correspond to the areal rainfall ($R_a|R_r=r$). These generated values can then be used to provide the desired estimates of the conditional distributions of the true area-averaged rainfall, $f(R_a|R_r)$, conditioned on RR. They can be applied to reconstruct the bivariate distribution of RR and the corresponding true areal rainfall based on the following formula:

$$f(R_a, R_r) = f(R_a|R_r)\, f(R_r)\ , \tag{14}$$

which can then be used to identify the PQPE model at different spatiotemporal scales as outlined in the previous Section of this report.

B.4.2.2. *Tests of the CDT Method*

The goal of the point-area transformation scheme is to obtain the estimates of conditional probability distributions of the true areal rainfall, conditioned on RR values, based on the conditional distributions of rain gauge rainfall and information on the conditional spatial correlation in the rain-field.

To evaluate the performance of the CDT method we used the data sample of point rainfall, areal rainfall and the corresponding RR estimates over three testing boxes within the USDA Agricultural Research Service Micronet that are indicated in Figure 3.

Only one time scale of 15 minutes was considered at this stage. We stratified the sample into sub-samples of four intervals of the 15-minute RR values, R_r. For each sub-sample separately, we carried out the following procedure:

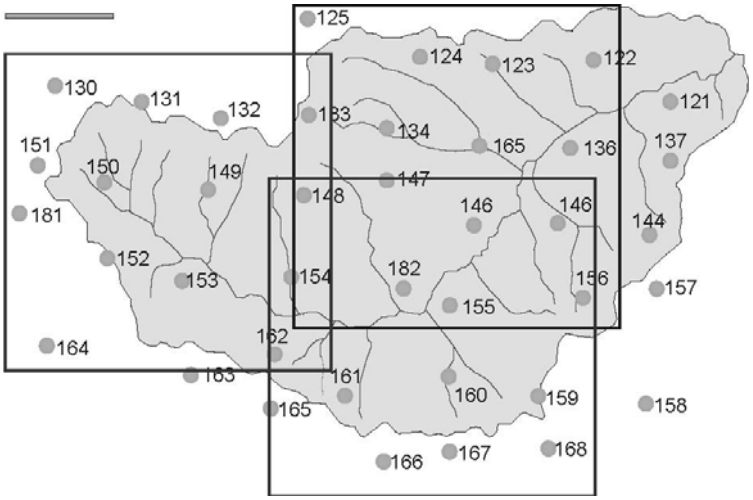

Fig. 3. A layout of the Little Washita Micronet with the three rectangular areas of about 19 km by 18 km that are used for testing the CDT method. Rain gauges within each area provide approximations of the true areal rainfall.

1. Construct the sample of concurrent point and areal rainfall for a specified spatiotemporal scale. The R_a values are approximated by averaging the rain gauge observations within the area of interest, whereas the R_p values come from all the individual gauges.

2. Estimate the sample variances of the point and areal rainfall values. Estimate the Hermite expansion coefficients for the point rainfall and the value of the scaling coefficient.

3. Perform the distribution transformation procedure described in section 2 to retrieve the areal rainfall distribution.

4. Compare the retrieved areal rainfall distribution against the observed one.

The estimates of the scaling coefficient, a, assumed values of about 0.6, for each of the sub-samples. The conditional quantile-quantile plots resulting from these tests are shown in Figure 4.

The solid dots in the plots show the comparisons of the quantiles corresponding to the same probability of exceedence for the transformation-based rainfall distributions as a function of the gauge-averaged (approximating the true areal) rainfall distributions. The open circles in the plots show the comparisons of the corresponding quantiles for the single-gauge rainfall distributions as a function of the gauge-averaged rainfall distributions. The transformation-based distributions are in a good agreement with the observed conditional distributions of areal rainfall and the degree of improvement of the radar rain gauge comparison can be seen from the comparison with the single rain gauge rainfall distributions. The tests confirm that the CDT method is able to retrieve the conditional distributions of the areal rainfall with quite good degree of accuracy.

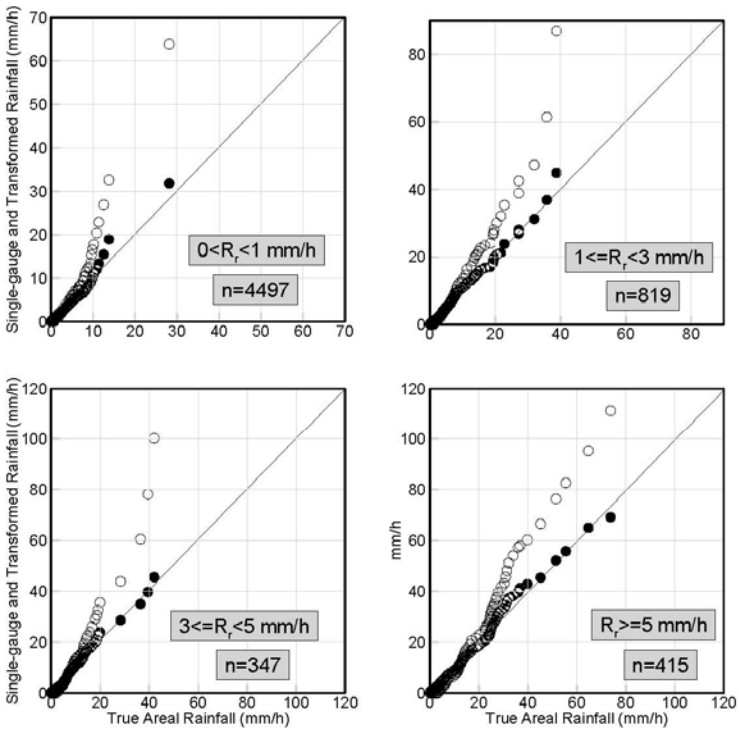

Fig. 4. A quantile-quantile plot of the cumulative rainfall distributions conditioned on the radar rainfall. Filled circles correspond to the transformation-based versus the true areal rainfall distributions. Open circles correspond to the point (single-gauge) versus the true areal rainfall distributions. The sample was stratified into four ranges of RR estimates. In the plots, n refers to the sample size in each range.

B.4.2.3. *Discussion*

The conditional scaling factors in the CDT method and their dependence on the spatial averaging scale are determined only by the distributions and the spatial correlation functions of the radar-conditioned rain gauge rainfall. These quantities are, in principle, measurable and no other fundamental assumptions are necessary to use the CDT in practical applications. However, successful application of the CDT method requires sufficiently accurate information on the rainfall spatial correlation structure conditioned on the radar estimates over the spatial scales below the resolution of the RR product. This information is available in many situations where dense rain gauge clusters exist within the sparse networks (e.g., in Oklahoma, or Iowa). Of course, the estimates of spatial correlation are bound to be uncertain. The effects of these uncertainties on the CDT scheme are complex and their quantification remains to be investigated. However, one thing that we can be sure of is that, whatever are the uncertainties in the conditional correlations, the CDT always reduces the RR uncertainty bounds in comparison

with what we could obtain if we treated the single-gauge data as the corresponding truth. By its mathematical nature, the CDT just cannot increase the estimated RR uncertainty bounds. Of course, these RR uncertainty estimates are also not perfectly accurate, but this gauge-error filtering method always corrects them in the right direction. The effectiveness of this correction is clearly demonstrated in Figure 4 by comparison of its results and the single-gauge performance. As one can see, the departures from the one-to-one line for the CDT transformed and the true area-average rainfall distributions are about ten times smaller than the discrepancies between the single-gauge and true area-average rainfall distributions. Error reduction by an order of magnitude is a very good performance for a relatively simple statistical method.

C. DATA ANALYSES

Development and testing of the above described PQPE framework requires massive radar and rain gauge data sets. As we argued in Krajewski and Ciach (2003) and Krajewski et al. (2003), for the PQPE algorithm to be meaningful it must be strongly based in empirical data. Fundamentally, two data types are required for this: (1) radar-rainfall estimates and (2) rain gauge data. While the PED approach relies on radar-rainfall products, it is important to begin with basic radar volume scan data. This way the calculated products are consistent. For the rain gauge data the basic issue is data quality (e.g. Steiner et al. 2000). Below we discuss our progress thus far in data collection and preparation.

C.1.1. Preparation of the Large Data Sample

To facilitate our studies we compiled a large sample of Level II radar reflectivity data acquired from the National Climatic Data Center (NCDC) for the Oklahoma City NEXRAD WSR-88D site (KTLX). The current sample covers the six-year period from January 1998 to December 2003. We used the Level II data as input to Build 4 of the Open Radar Product Generator (ORPG) Precipitation Processing System (PPS) software system and generate the Digital Precipitation Array (DPA) products which represent one-hour accumulations and are given on the Hydrologic Rainfall Analysis Project grid (Reed and Maidment 1999). For rain gauge data we use observations from three networks: (1) the Oklahoma Mesonet (we acquired the data from the JOSS Office in support of another NOAA-sponsored project); (2) the USDA Agricultural Research Service (ARS) Micronet (we acquired the data through the OHD), and (3) the University of Oklahoma Environmental Verification and Analysis Center (EVAC) Piconet located at the Oklahoma City International Airport (we established and maintained the network ourselves). We described these data sets in more detail below.

C.1.1.1. *The 6-year Sample of the KTLX Data*

This sample consists of about 350,000 data files and contains radar observations collected during the years of 1998-2003. We converted the files from the standard UNIX compression format that is still used by the NCDC to the much more efficient “bzip” format that is currently used as a standard by the OHD. We decided to adapt to this standard for its speed and efficient use of disk space.

We performed a quality check of all the files which revealed occasional errors in the file structure. About 7,000 (or 2%) of the files are affected by these errors. The impact of these errors on the automatic ORPG data processing has been tested and discussed with the OHD specialists. We excluded these suspect files from further processing.

C.1.1.2. *Oklahoma Mesonet Data*

The Oklahoma Mesonet (Brock et al. 1995) is known as perhaps the best regional network of surface meteorological sensors in the country. The stations are fairly uniformly distributed over the state and thus the data cover the full range of distances from the KTLX radar.

The Mesonet rainfall data are provided as cumulative values, reset at the beginning of each day. For this dataset, a flagging system is associated with the data to indicate data quality. While preprocessing the data and organizing them as 5-minute rain gauge rainfall, we found about 100 entries of negative accumulation that were erroneously flagged as good quality data. We reported these cases to the Oklahoma Mesonet's quality-assurance team and they manually flagged these cases in their database. Based on our input they investigated the causes of the bad data and decided to reprocess their entire data set. They will provide the data to us as soon as the reprocessing is completed (probably around June 20th).

Within the KTLX umbrella, there are about 100 rain gauges, almost uniformly distributed, covering a wide range of distances (from about 25 km to the edge of the radar umbrella). Four of the Mesonet stations are within or very close to the Micronet network. The information obtainable from the flags in these Mesonet stations could be useful during the QC of the Micronet data.

C.1.1.3. *ARS Micronet Data*

We acquired the corresponding rain gauge data through the OHD. We received the 5-minute rain gauge accumulation data for 42 stations covering the Little Washita watershed located about 90 km south-west from the KTLX WSR-88D site (see Figure 5). One limitation of the analysis based on this ground reference is that it covers only a very limited range of the distances from the radar (from about 70 km to about 105 km).

The original ARS Micronet archive is organized in a very inefficient way and consists of about 640,000 small files. In addition, the timing convention in this archive is incompatible with our radar data. To make the data usable, we preprocessed the entire archive and converted it to 72 monthly files of the 5-minute rain gauge rainfall. During this preprocessing, we detected several errors in the data. These errors were corrected, whenever possible, or flagged as missing data records.

The ARS Micronet data we were provided did not have quality control (QC) flags. At this stage, we have not yet performed extensive QC on the rain gauge data. However, while organizing the data in 5-minute rain gauge rainfall, we checked for negative accumulations and we found more than 20 of such entries. We also found a case where high rainfall was detected by only one station but no rain was collected by any other gauge for few hours before and after. We have corrected these errors, whenever possible, or flagged them as missing data records.

Once organized the dataset in a more efficient way, we have georeferenced the rain gauges to the HRAP grid, and extracted the corresponding and collocated radar values. We have then accumulated the rain gauge rainfall to hourly scale to have the same temporal resolution of the RR estimates.

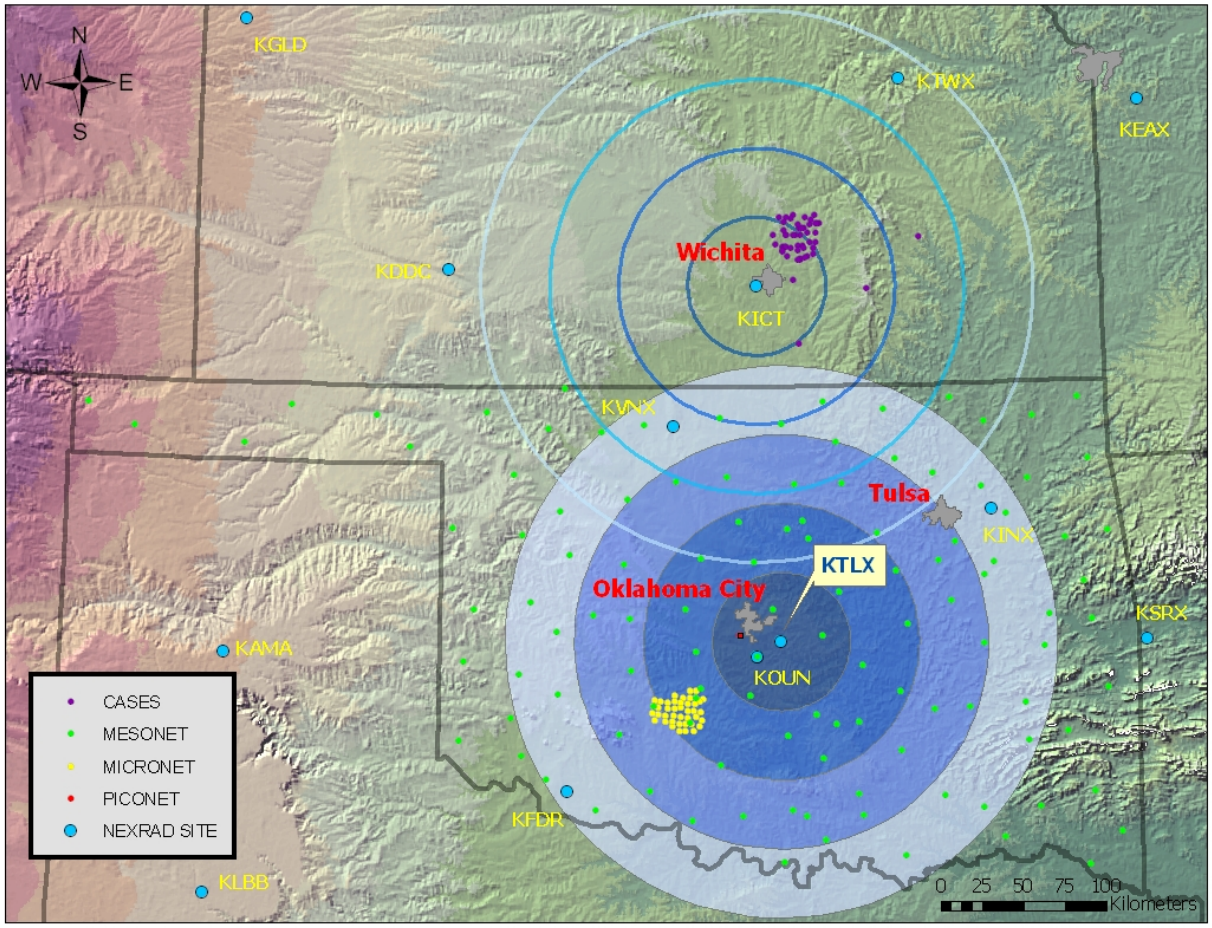

Figure 5. Schematic map of the Oklahoma/Kansas area and the relevant rain gauge networks. (We did not use data from the CASES network in this study.)

C.1.1.4. *Oklahoma Piconet Data*

To be completed.

C.1.2. Basic Data Characteristics

C.1.2.1. *Seasonal Partitioning*

Since it is well known that seasonal variability strongly affect the uncertainty of radar-rainfall products, we performed a simple analysis of data to determine a possible division of the sample into adequate periods that are more homogeneous in terms of their statistical characteristics. As an index, we used the rain-weighted temperatures (T_{rw}) for each month, defined as:

$$T_{rw} = \frac{\sum_i R_i T_i}{\sum_i R_i}, \tag{15}$$

where R_i and T_i are the rainfall and temperature measured at the i^{th} station.

Figure 6 shows the monthly T_{rw} averaged over the six years of data. Based on this plot, we have decided to divide the dataset into three season: cold (January, February, March, November and December), where the average T_{rw} is below or around 10°C; warm (April, May and October), where the average T_{rw} is between 15 and 20°C; hot (June, July, August, September), where the average T_{rw} is above 20°C.

In Figure 7 a different characteristic distribution of the rain-wighted temperature is evident: the cold season is positively skewed, the warm season is more symmetrical, while the hot season is negatively skewed.

C.1.2.2. *General Data Features*

Figure 8 shows the time series of the monthly accumulation from gauge and radar estimates. It is possible to notice how the radar tends to have larger values than the rain gauge. This feature is more evident from Figure 9, where, for most of the months, the value of the bias is smaller than 1. It seems that, for some months, the value of the bias is very large. However, looking at Figure 8, it is possible to notice how these cases correspond to months with low accumulation. Overall, there is good agreement between radar and gauge estimates, as illustrated by high correlation coefficient values (Figure 10).

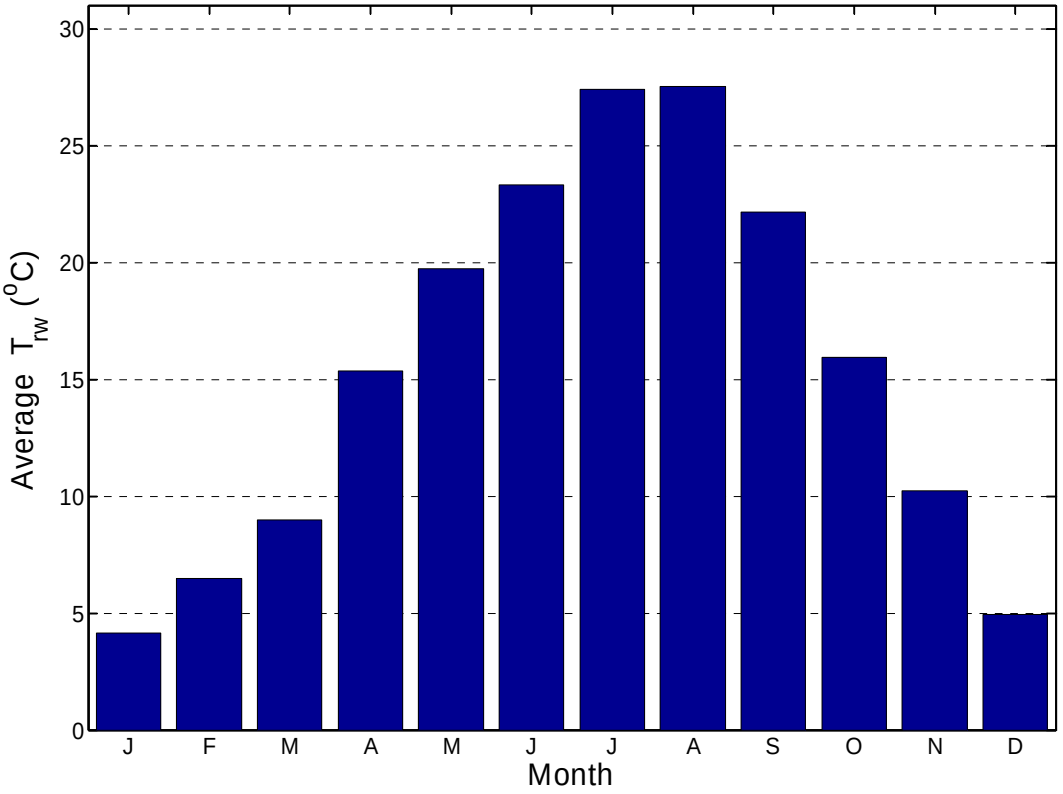

Fig. 6. Histogram of the rain-weighted temperature (T_{rw}) according to month, averaged over the six-year period under study.

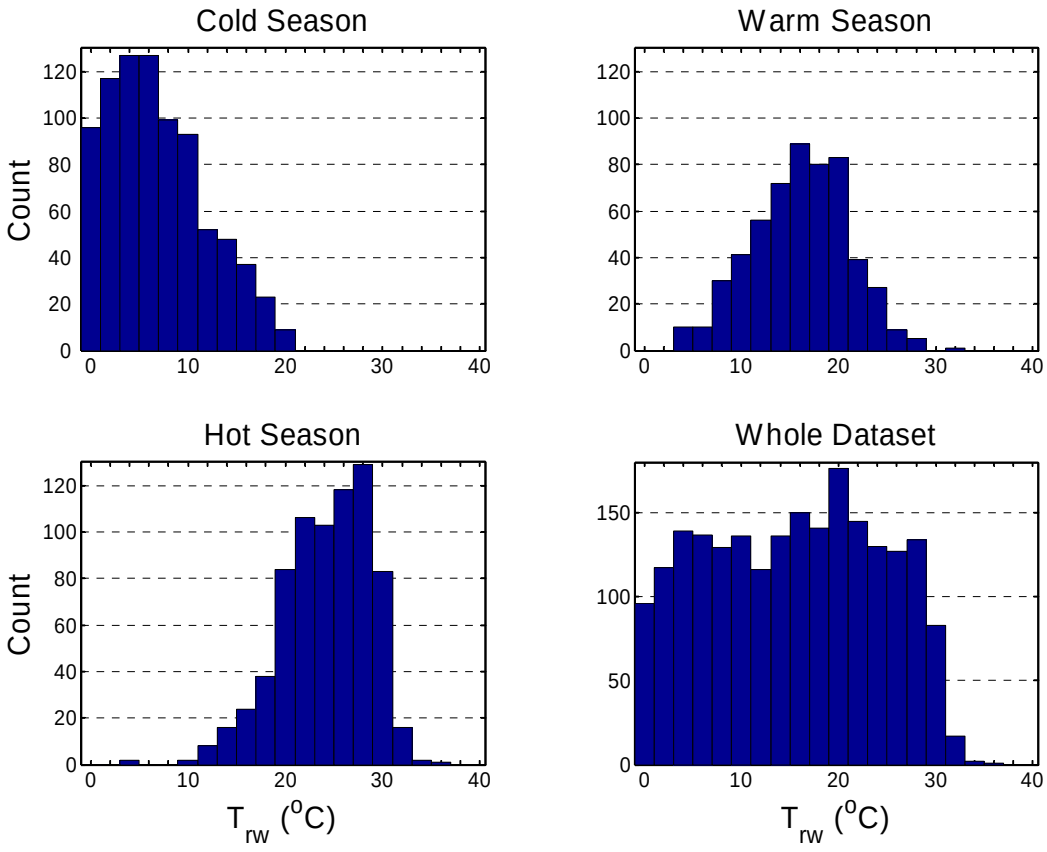

Fig. 7. Histogram of the rain-weighted temperatures (T_{rw}) for the three seasons and for the entire dataset. Each of the seasons is characterized by a different behavior: the cold season is positively skewed, the warm season is more symmetrical while the hot season is negatively skewed.

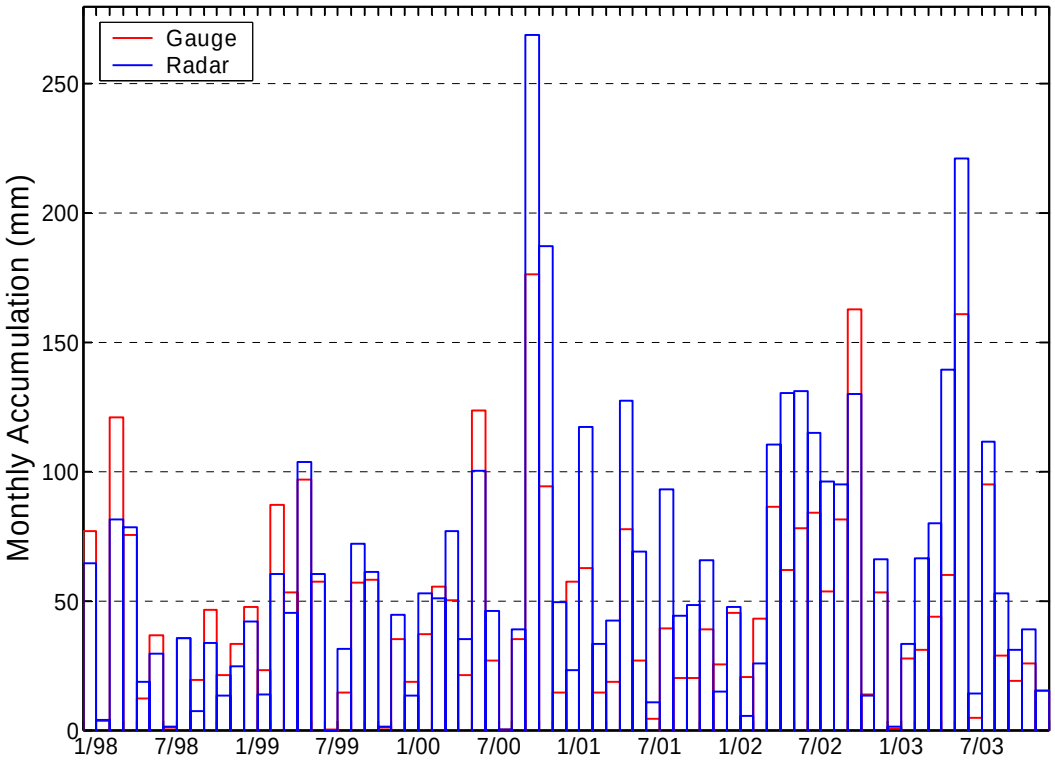

Fig. 8. Time series of the monthly accumulation for the rain gauges and the radar for the six-year study period. These values have to be considered as an underestimation of the true value because of the missing data.

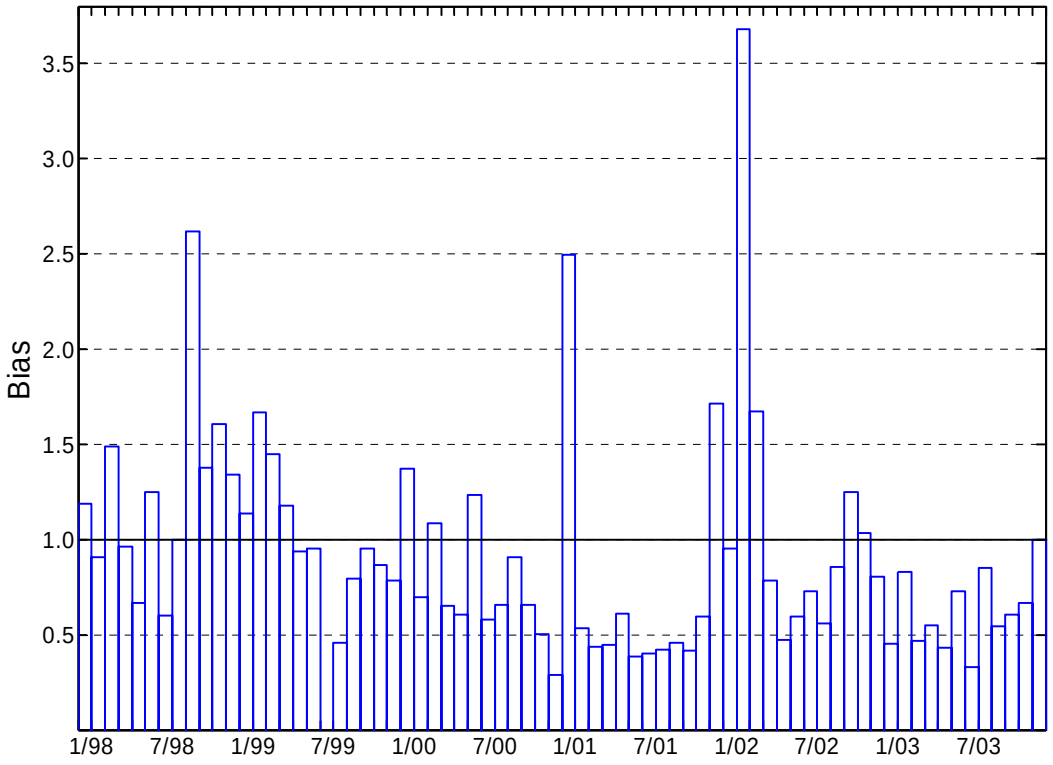

Fig. 9. Time series of the bias for the 6-year period under study.

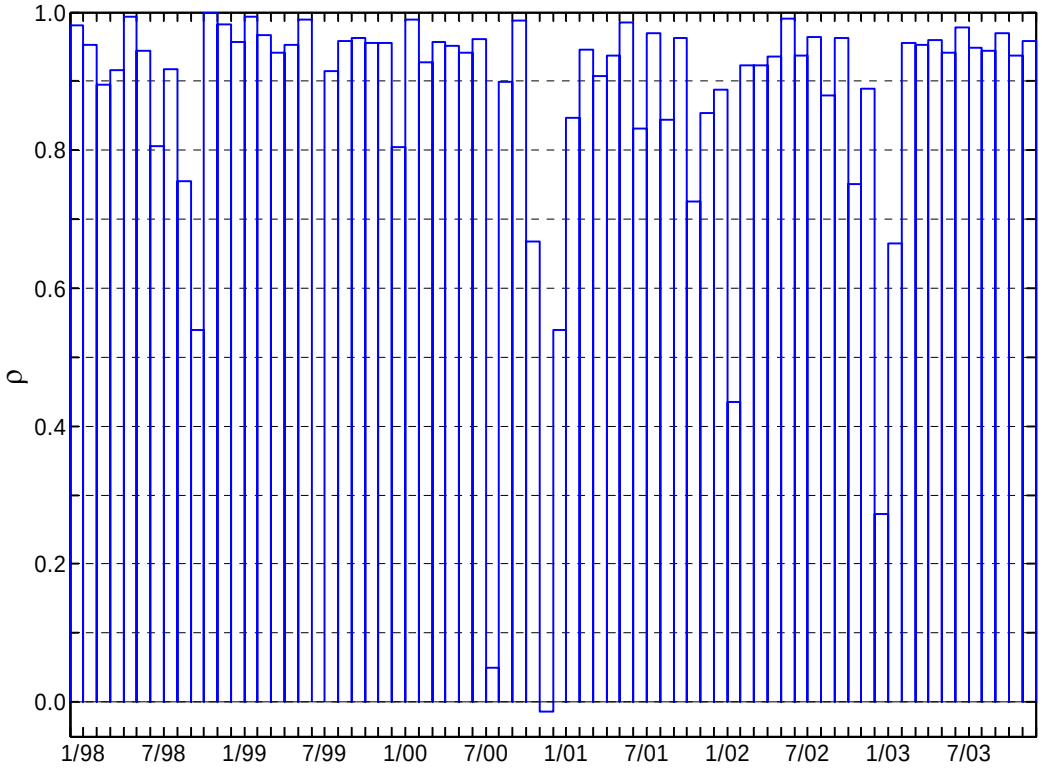

Fig. 10. Time series of the correlation coefficient ρ between rain gauge and radar data for the six-year period under study. It is possible to notice values of ρ higher than 0.8 for most of the months, meaning that there is a good linear relationship between radar and rain gauge data.

Figures 11 and 12 show the correlations and the correlation function estimated from the rain gauge rainfall and the collocated RR estimated for the hourly time scale. We have chosen a three-parameter exponential model:

$$\rho(d) = \theta_0 \exp\left[-\left(\frac{d}{\theta_1} \right)^{\theta_2} \right] \tag{15}$$

where d is the separation distance, θ_0 is the correlation at $d = 0$, θ_1 the correlation distance and θ_2 the shape factor. The parameters have been obtained through a global grid search, where we minimized the root mean squared error, with a resolution of 0.01 for θ_0, 0.1 km for θ_1 and 0.01 for θ_2. It is possible to notice how θ_1 is always bigger for the gauge correlation, with the exception of the hot season. These results are in agreement with those by Gebremichael and Krajewski (2004). In the same figures, we have also plotted the correlation function estimated for the EVAC Piconet network (Ciach and Krajewski 2005). It would be extremely useful to integrate the information at the small-scale from Piconet network (gauge separation distance smaller than 4 km) with the information at the larger scale (gauge separation distance larger than 4 km) from Micronet and Mesonet networks.

As mentioned before, the ARS Micronet is located between 70 and 105 km from the radar site. Figure 13 shows how, within this range, the correlation coefficient ρ is above 0.8 for the whole dataset and the warm and hot season, while for the cold season it is below. In all of the plots there is a slight tendency for the correlation to decrease for increasing distance. Similar feature can be observed for the bias (Figure 14). In this case, all of the plots have bias values smaller than 1.

From the plots of correlation and bias as a function of the distance from the radar site, it is possible to notice how a couple of stations seem to behave differently when compared to the general pattern. This information is useful for quality control.

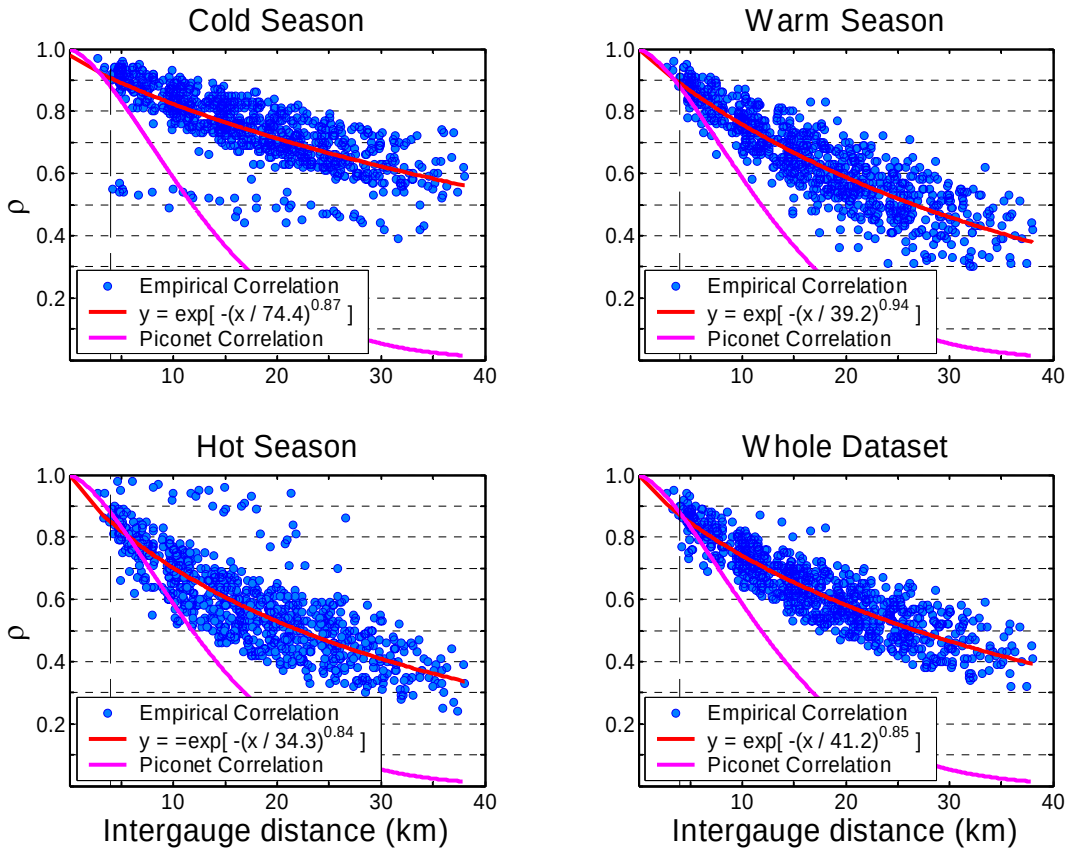

Fig. 11. Spatial correlation of the Micronet rain gauges for the three seasons and the whole dataset. The solid red lines are obtained fitting the data with a three-parameter exponential function; the solid magenta line is from the spatial correlation function estimated by Ciach and Krajewski (2005) for the Piconet rain gauge network and the vertical dashed line corresponds to its largest intergauge distance.

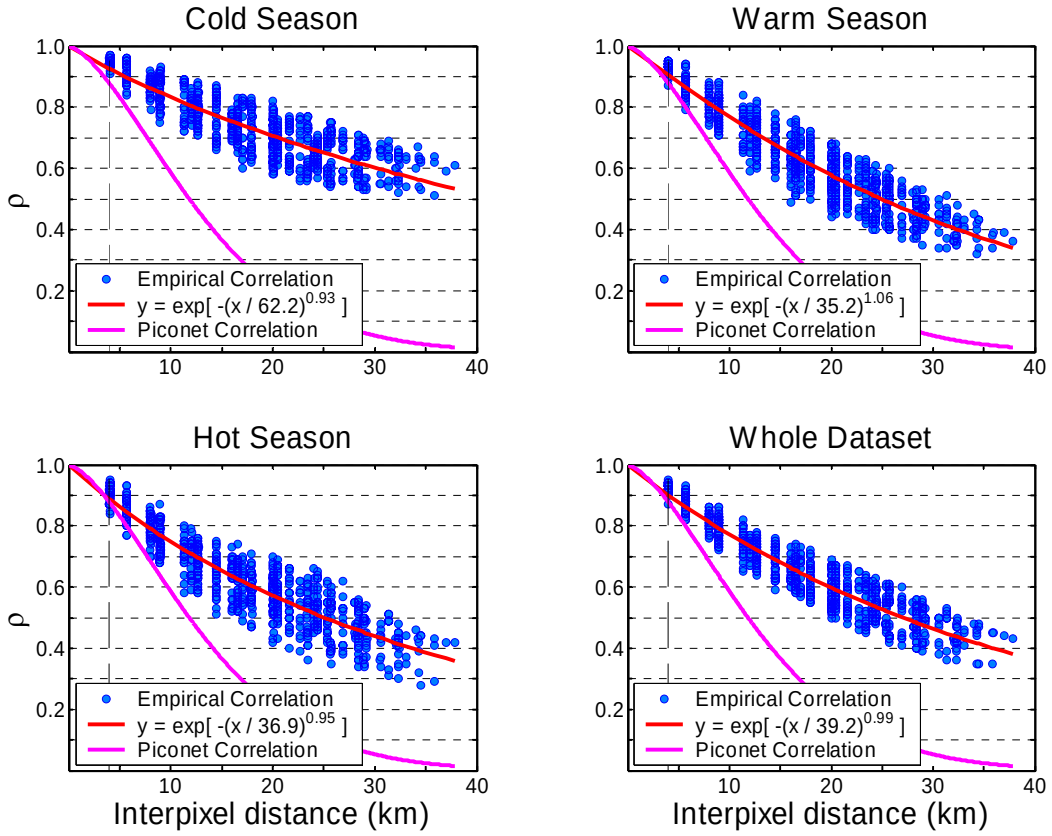

Fig. 12. Spatial correlation of the radar data at the locations of the Micronet rain gauges for the three seasons and the whole dataset. The solid red lines are obtained fitting the data with a three-parameter exponential function; the solid magenta line is from the spatial correlation function estimated by Ciach and Krajewski (2005) for the EVAC Piconet rain gauge network and the vertical dashed line corresponds to its largest intergauge distance.

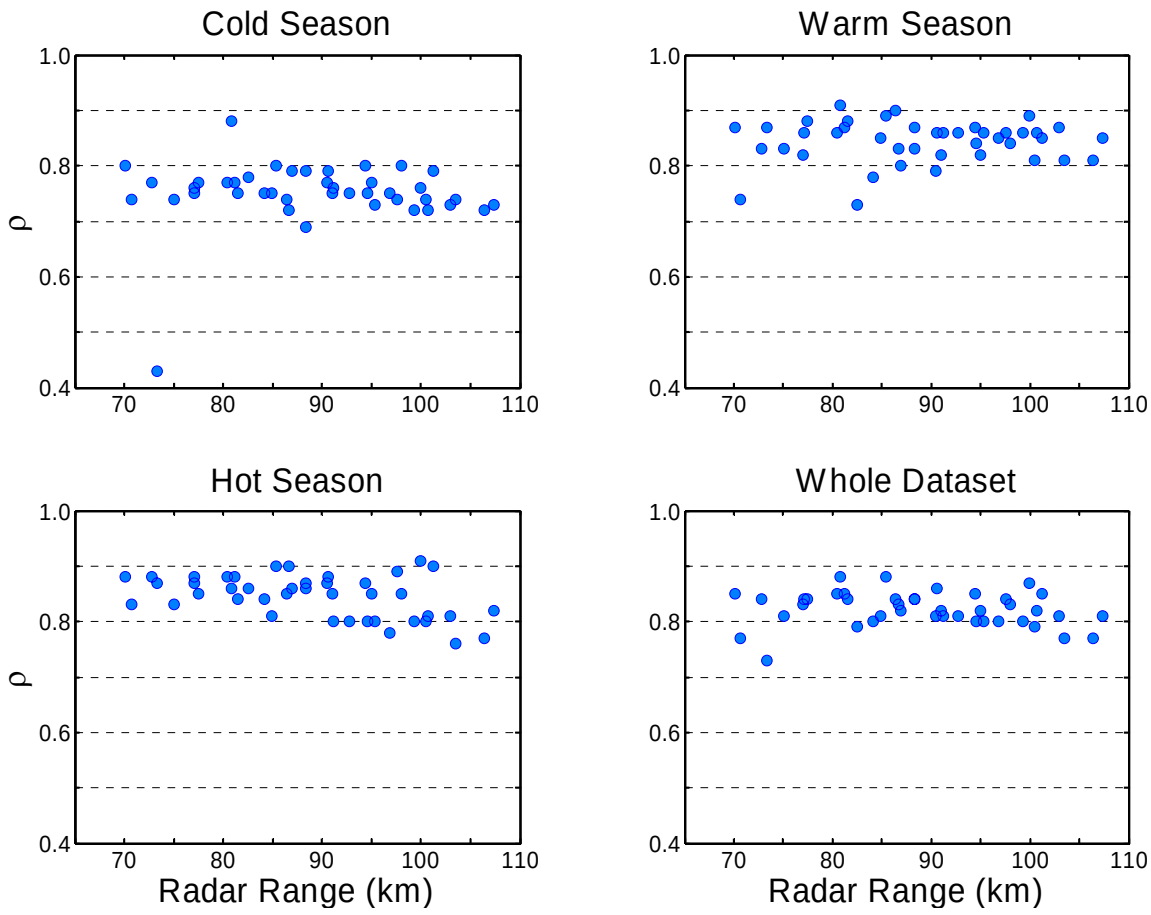

Fig. 13. Correlation coefficients between rain gauge and collocated radar values estimated from the Micronet network as a function of the distance from the radar site.

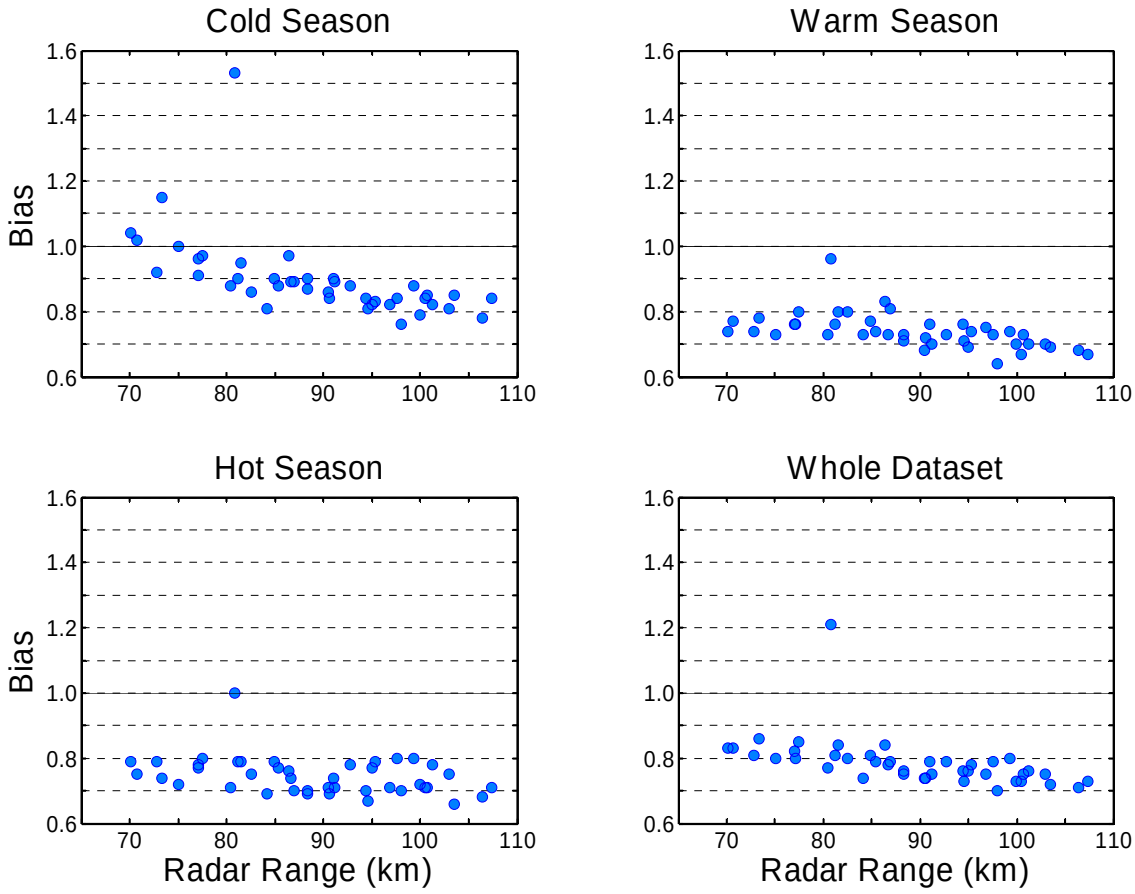

Fig. 14. Bias estimated from the Micronet network as a function of the distance from the radar site.

C.1.2.3. *Overall Bias*

Before estimating the deterministic and the random components, we have removed the bias from the radar data:

$$bias = \frac{\sum_{i=1}^{n} G_i}{\sum_{i=1}^{n} R_i} \tag{16}$$

where G_i is the rain from the i^{th} gauge and R_i is the corresponding value from the radar. According to our partitioning, we have four different values, three for the three seasons and one for the entire dataset:

- Cold season: 0.90
- Warm season: 0.75
- Hot season: 0.72
- Whole dataset: 0.78

According to the definition of bias, it means that there is an overall overestimation by the radar, more evident during the warm and hot seasons. It is difficult to ascribe it to a specific reason (e.g. radar miscalibration); in addition, we do not have to forget that the rain gauge data have not yet been quality controlled.

C.1.3. Conditional Analyses

C.1.3.1. *Outline of the Nonparametric Procedure for Conditional Analysis*

As mentioned before, to characterize the relation between radar-rainfall (RR) and the true rainfall, it is possible to consider the true rainfall (RA) as the product of a deterministic distortion function $h(\cdot)$ of the RR and of the random uncertainties $e(\cdot)$:

$$R_a = h(R_r) \cdot e(R_r) \tag{17}$$

where R_r and R_a represent the corresponding (concurrent and collocated) RR and RA. This relation has the flexibility to account for different spatio-temporal scales, distance from the radar and synoptic conditions.

To identify the model, it is necessary to estimate the deterministic function $h(\cdot)$ and the statistical distribution of the random component. At the present stage, we have used only the information from the ARS Micronet network.

Once removed the overall bias, we have defined the deterministic component $h(r_r)$ as the following conditional expectation:

$$h(r_r) = E[R_a \mid R_r = r_r] \qquad ()$$

The deterministic component can be approximated using a nonparametric regression method (Hardle 1990; Simonoff 1996). In this study we have used the following moving-window averaging:

$$h(r_r) = \left. \frac{\sum_i (w_i R_{a,i})}{\sum_i w_i} \right| \frac{r_r}{k} \le R_r \le r_r k \qquad ()$$

where:

k is a parameter that regulates the size of the moving window centered on $R_r = r_r$. The size of the windows linearly increases with r_r so that a reasonable number of data points are used for the estimation. For this study, k is set equal to 1.5.

w_i is the weighting factor and it is computed as:

$$w = 1 - \left(\frac{\log \frac{R_r}{r_r}}{\log k} \right)^2 \qquad ()$$

It is equal to 1 for $R_r = r_r$ and it decreases moving far from the center of the window.

Once we have estimated the deterministic component, we are able to characterize the random errors $e(R_r)$ in the multiplicative and additive forms:

$$e(R_r) = \frac{R_a}{h(R_r)} \qquad ()$$

$$e(R_r) = R_a - h(R_r) \qquad ()$$

From these formulations, it is possible to notice that the conditional expected values of $e(\cdot)$ are always equal to:

$$E\left[e \mid R_r = r_r\right] = 1 \qquad \text{(multiplicative form)}$$

$$E\left[e \mid R_r = r_r\right] = 0 \qquad \text{(additive form)}$$

while the standard deviations of the random component $\sigma_e(r_r)$ depends on RR estimates:

$$\sigma_e(r_r) = \sqrt{\frac{1}{N}\sum_{i=1}^{N}\left(\frac{R_a}{h(r_r)} - 1\right)^2} \qquad \text{(multiplicative form)}$$

$$\sigma_e(r_r) = \sqrt{\frac{1}{N}\sum_{i=1}^{N}\left[R_a - h(r_r)\right]^2} \qquad \text{(additive form)}$$

Using the same nonparametric approach described above, we have estimated $\sigma_e(r_r)$ as:

$$\sigma_e(r_r) = \sqrt{\frac{\sum_i\left[w_i\left(\frac{R_{a,i}}{h(r_r)} - 1\right)^2\right]}{\sum_i w_i}} \quad \frac{r_r}{k} \le R_r \le r_r k \qquad \text{(multiplicative form)}$$

$$\sigma_e(r_r) = \sqrt{\frac{\sum_i\left\{w_i\left[R_{a,i} - h(r_r)\right]^2\right\}}{\sum_i w_i}} \quad \frac{r_r}{k} \le R_r \le r_r k \qquad \text{(additive form)}$$

C.1.3.2. *Deterministic Component of the Error*

The deterministic distortion function h(□) describes all the systematic biases. We have estimated it using the aforementioned nonparametric framework for four different time scales (1, 3, 6, and 24 hours) for the three seasons and the whole dataset. Due to the way RR is estimated, we have not considered the whole dataset, but only the scans separated by at least 20% of the temporal resolution. In this way, we have more independent information.

Figures 15 and 16 show the results of analysis. It is possible to notice how the curves tend to be close to the 1:1 line, due to the removal of the overall bias, and then bend towards the x-axis. In the warm and hot seasons it seems that the curves follow the 1:1 line for a longer range. This can probably be attributed to the fact that there are more numerous smaller values in the cold season than in the warm and hot ones. For our analysis we have considered a minimum weighted sample size of 100. The vertical ticks mark the 1000 weighted sample size.

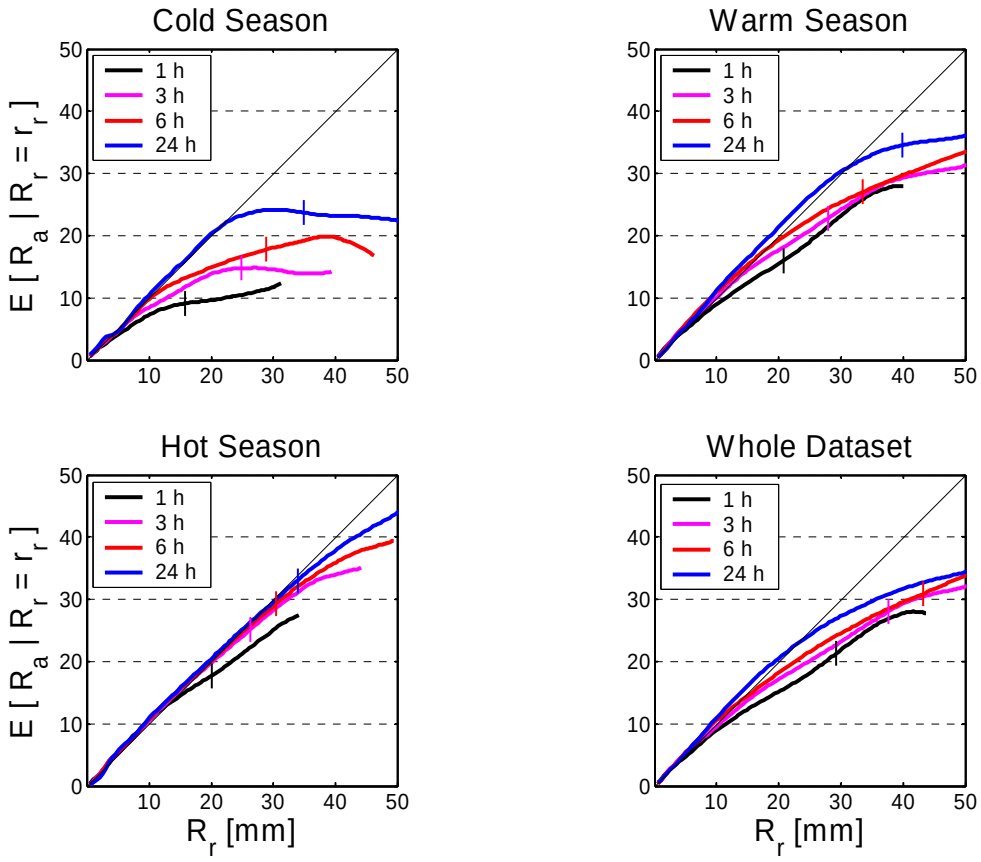

Fig. 15. Rain gauge averages, conditioned on radar rainfall values, after removing the overall bias for four time resolutions, for the three seasons and the whole dataset. The segments of the curves on the left of the vertical tick are computed using a weighted sample size larger or equal to 1000, while the segments on the right with a weighted sample size between 1000 and 100.

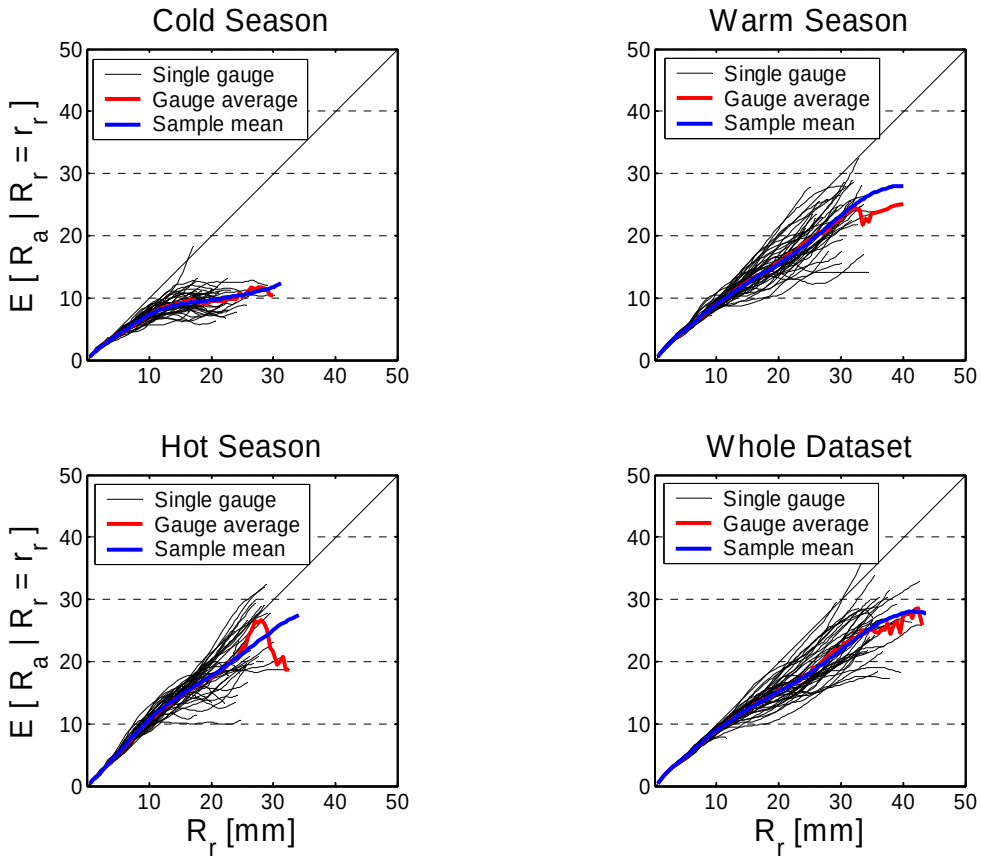

Fig. 16. Rain gauge averages, conditioned on radar rainfall values, after removing the bias for the hourly scale, for the three seasons and the whole dataset. The black lines correspond to individual gauges, the red line is obtained averaging each individual trace and the blue line is the sample mean (same as in Figure 15).

C.1.3.3. *Random Component of the Error*

The random component e(□) describes all random uncertainties. As mentioned before, it can be formulated in two ways, multiplicative or additive. Its mean does not depend on the RR values, while the standard deviation does. In Figure 17 we have plotted the standard deviation of the random component in the additive form, while in Figure 18 in the multiplicative form. In Figures 19 and 20 we show gauge by gauge results for hourly scale while in Figures 21-29 for 3-, 6- and 24-hour resolutions for the three seasons and the whole dataset. Comparing the results from the two formulations, it is possible to notice how the standard deviation in the multiplicative form for RR > 10 mm does not depend much on the temporal scale (with the exception of the cold season). This temporal invariance of e(□) in the multiplicative form will be very useful in the modeling effort.

To characterize the random component in terms of its statistical distribution, we have computed the 0.9, 0.75, 0.50, 0.25, and 0.25 quantiles, focusing our attention on the multiplicative form. As mentioned before, we know that its expected value is equal to 1 and does not depend on RR, while its standard deviation does.

Looking at the results for the three seasons and the whole dataset at the four time resolutions (Figures 30-33), it is possible to notice how the quantiles tend to be symmetrical with respect of the median. For this reason we have tried to model the empirical results with two symmetrical distributions (Gaussian and logistic) with mean equal to 1 and standard deviation equal to the standard deviation from the multiplicative formulation. The quantiles from these theoretical distributions fit quite well the empirical results (sometimes with the only exception of the cold season), especially for large values of RR. These results seem to support the error model proposed by Petersen-Øverleir (2005), who, even if using rain gauge data, perturbated his dataset with Gaussian-distributed deviates, justifying his choice with the Central Limit theorem.

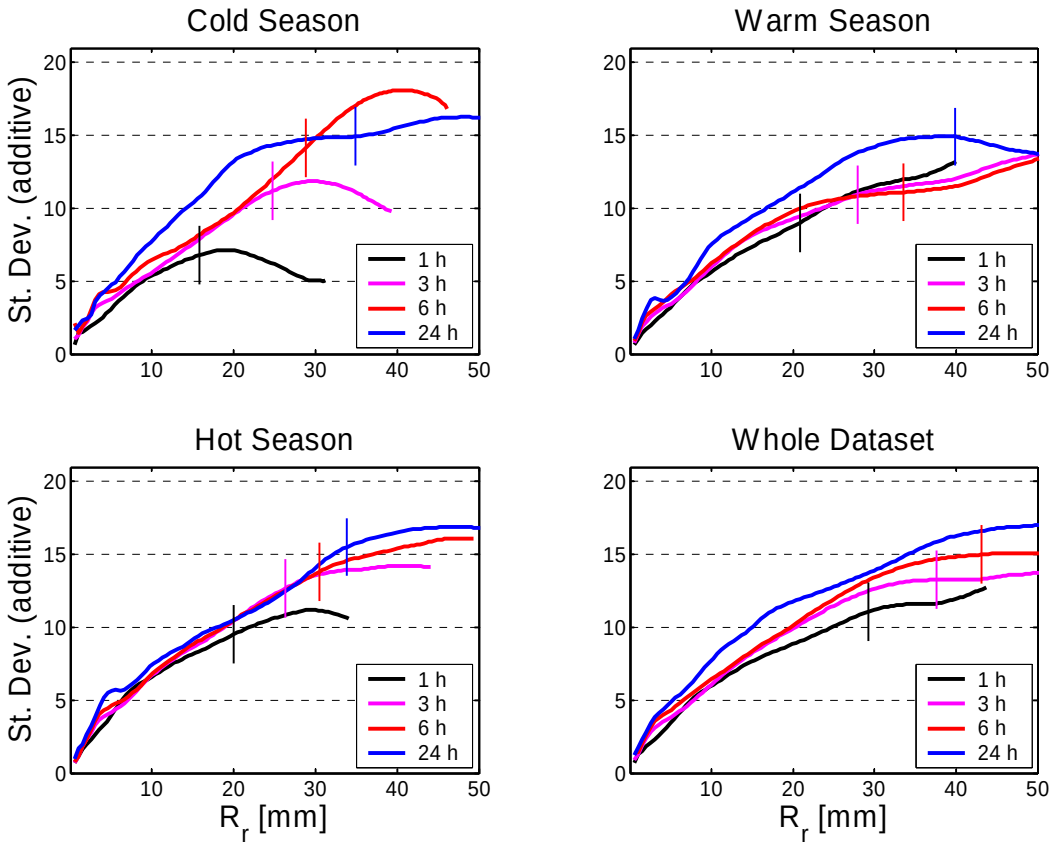

Fig. 17. Standard deviations of the random component in the additive form (mm) for the four temporal resolutions for the three seasons and the whole dataset. The segments of the curves on the left of the vertical tick are computed using a weighted sample size larger or equal to 1000, while the segments on the right with a weighted sample size between 1000 and 100.

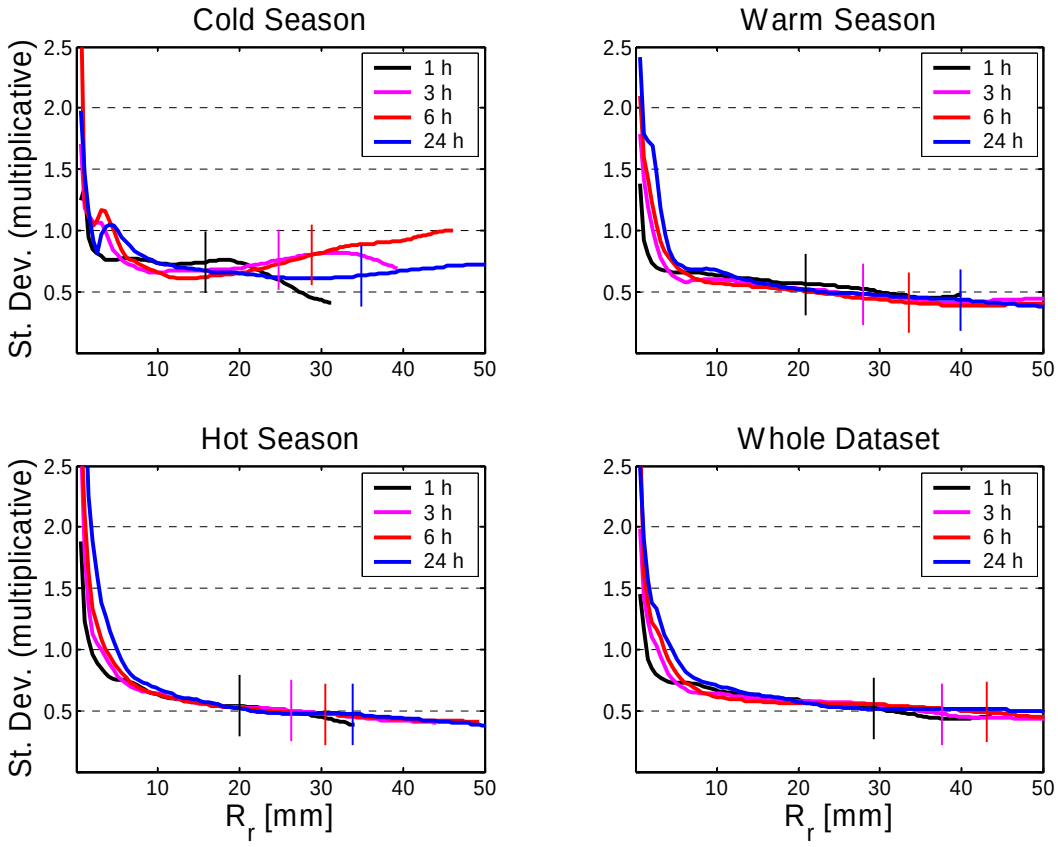

Fig. 18. Standard deviations of the random component in the multiplicative form (dimensionless) for the four temporal resolutions for the three seasons and the whole dataset. The segments of the curves on the left of the vertical tick are computed using a weighted sample size larger or equal to 1000, while the segments on the right with a weighted sample size between 1000 and 100.

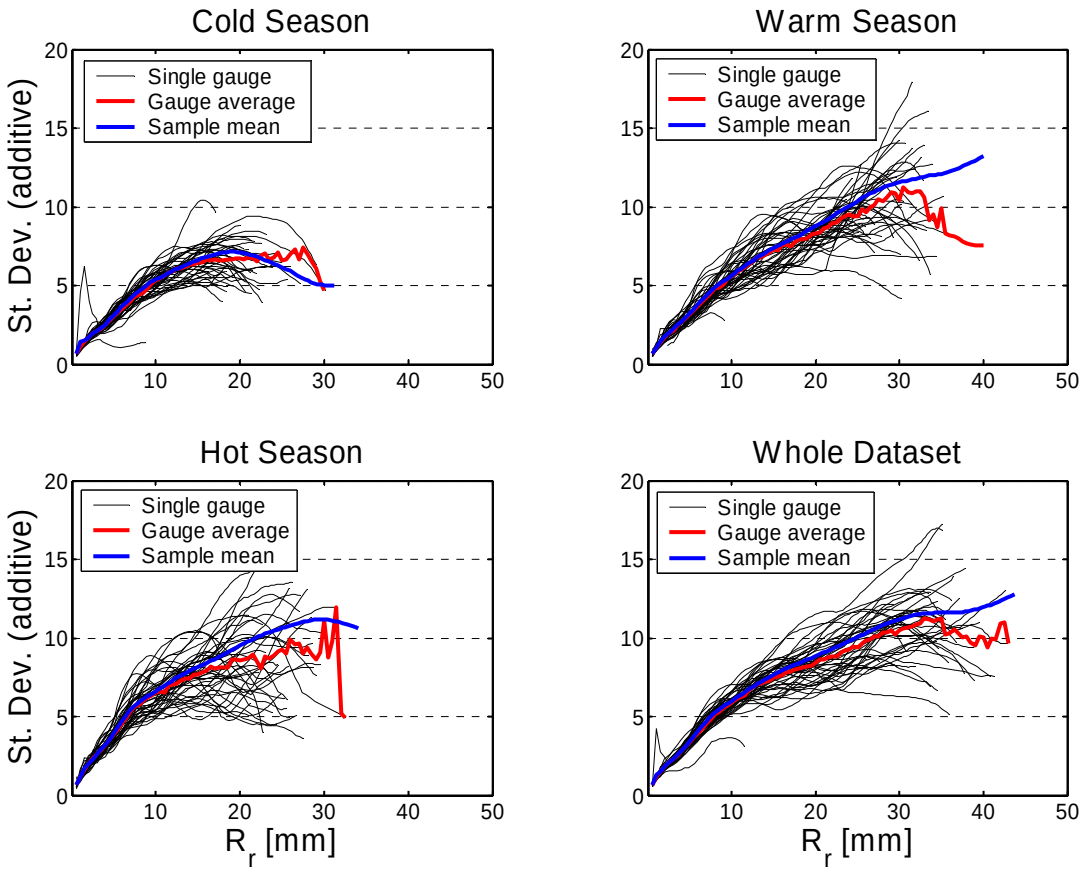

Fig. 19. Rain deviations of the random component in the additive form (mm) for the hourly scale, for the three seasons and the whole dataset. The black lines correspond to individual gauges, the red line is obtained averaging each individual trace and the blue line is the sample mean (same as in Figure 17).

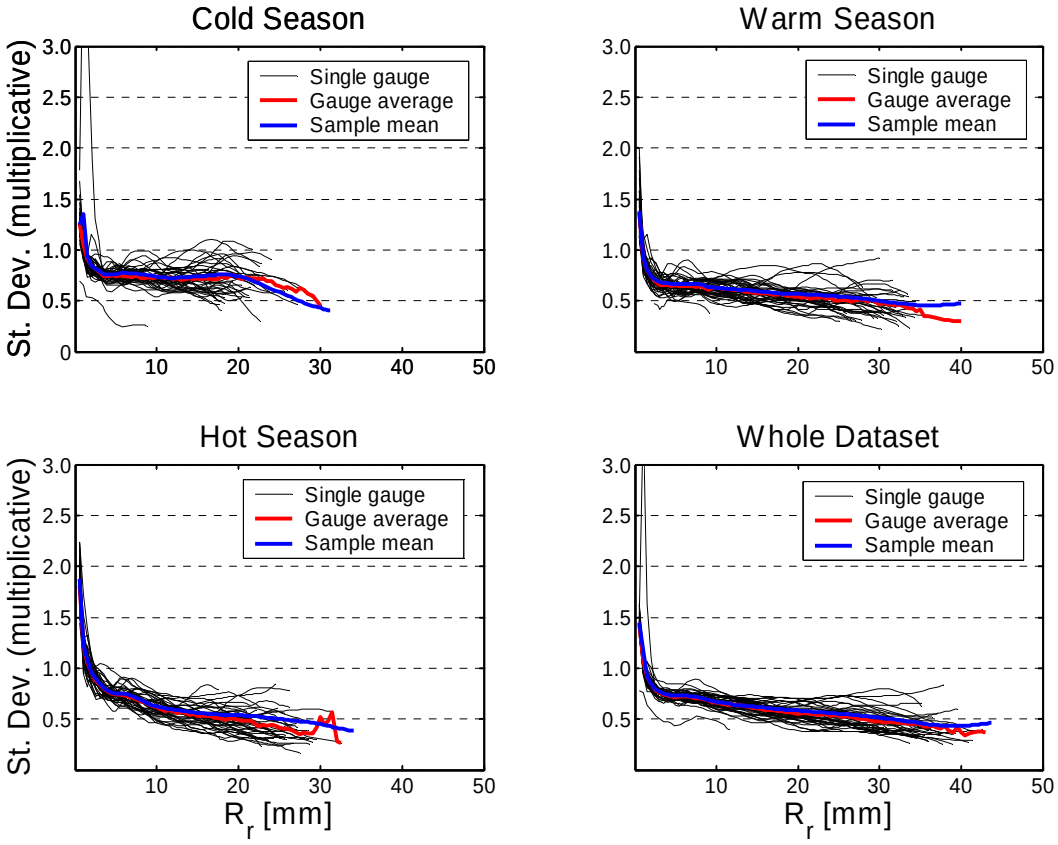

Fig. 20. Rain deviations of the random component in the multiplicative form (non-dimensional) for the hourly scale, for the three seasons and the whole dataset. The black lines correspond to individual gauges, the red line is obtained averaging each individual trace and the blue line is the sample mean (same as in Figure 18).

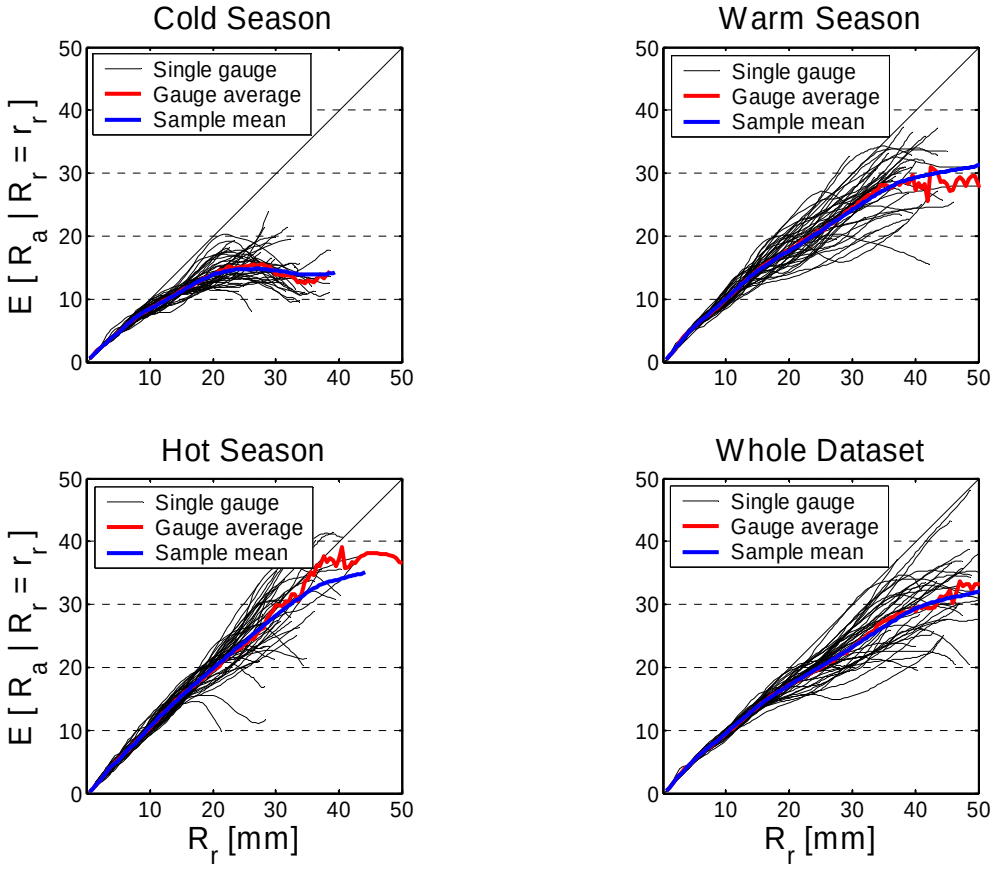

Fig. 21. Same as Figure 15, but for the 3-hour resolution.

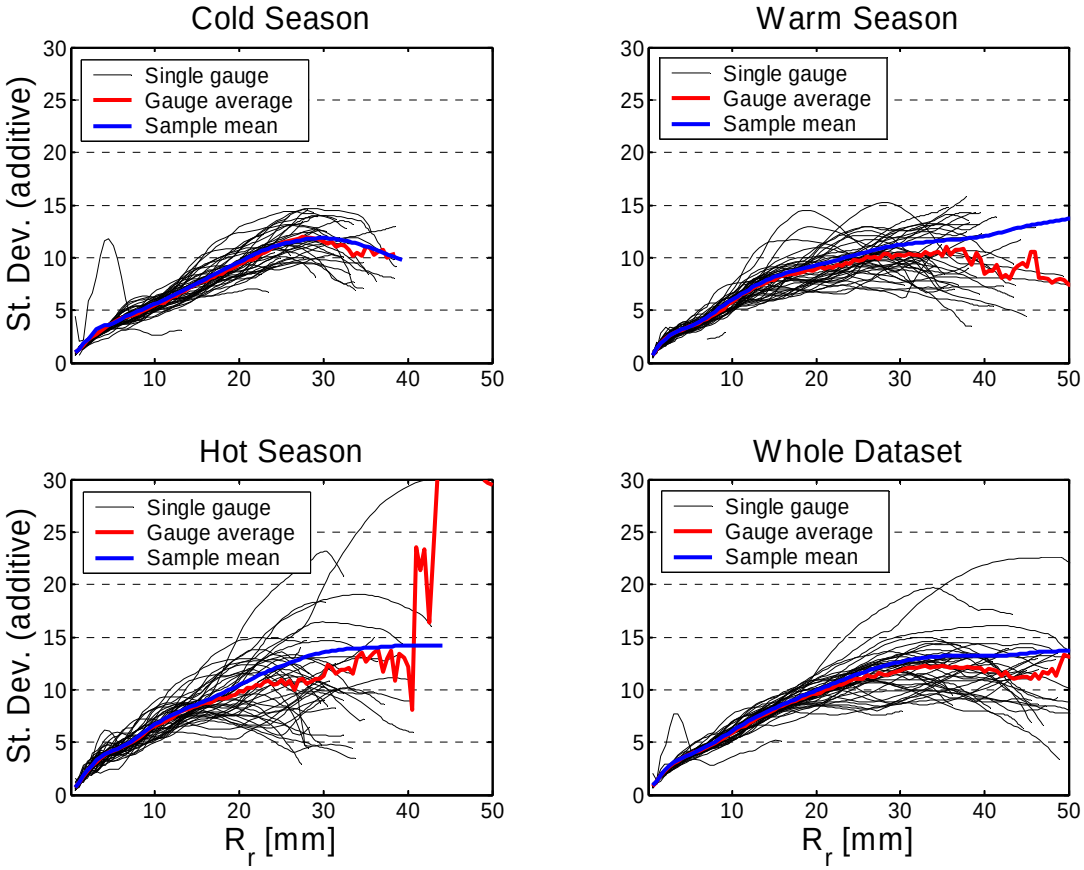

Fig. 22. Same as Figure 17, but for the 3-hour resolution.

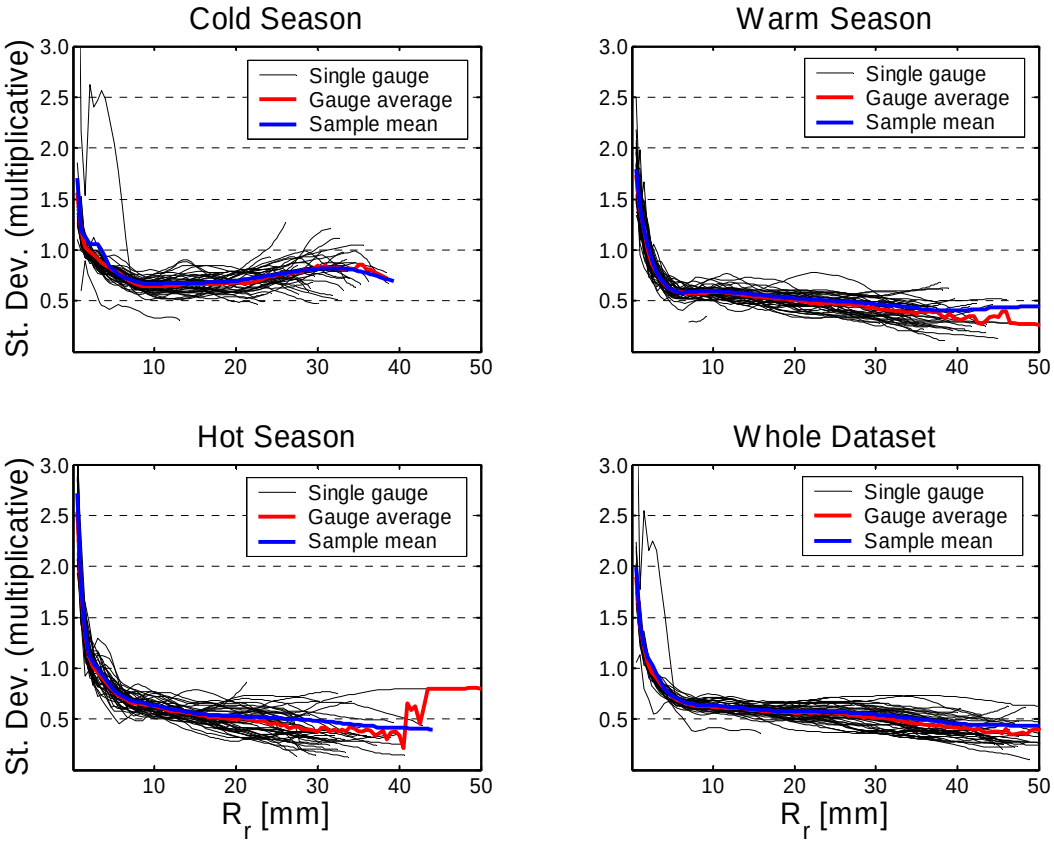

Fig. 23. Same as Figure 18, but for the 3-hour resolution.

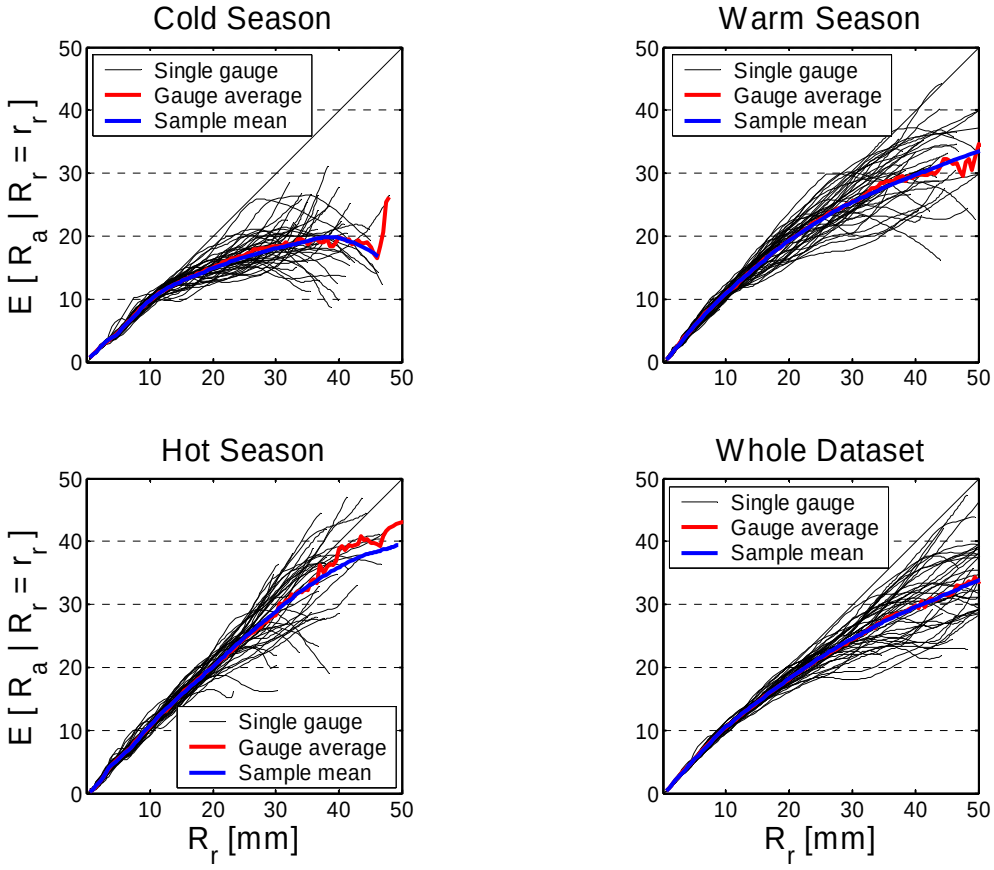

Fig. 24. Same as Figure 15, but for the 6-hour resolution.

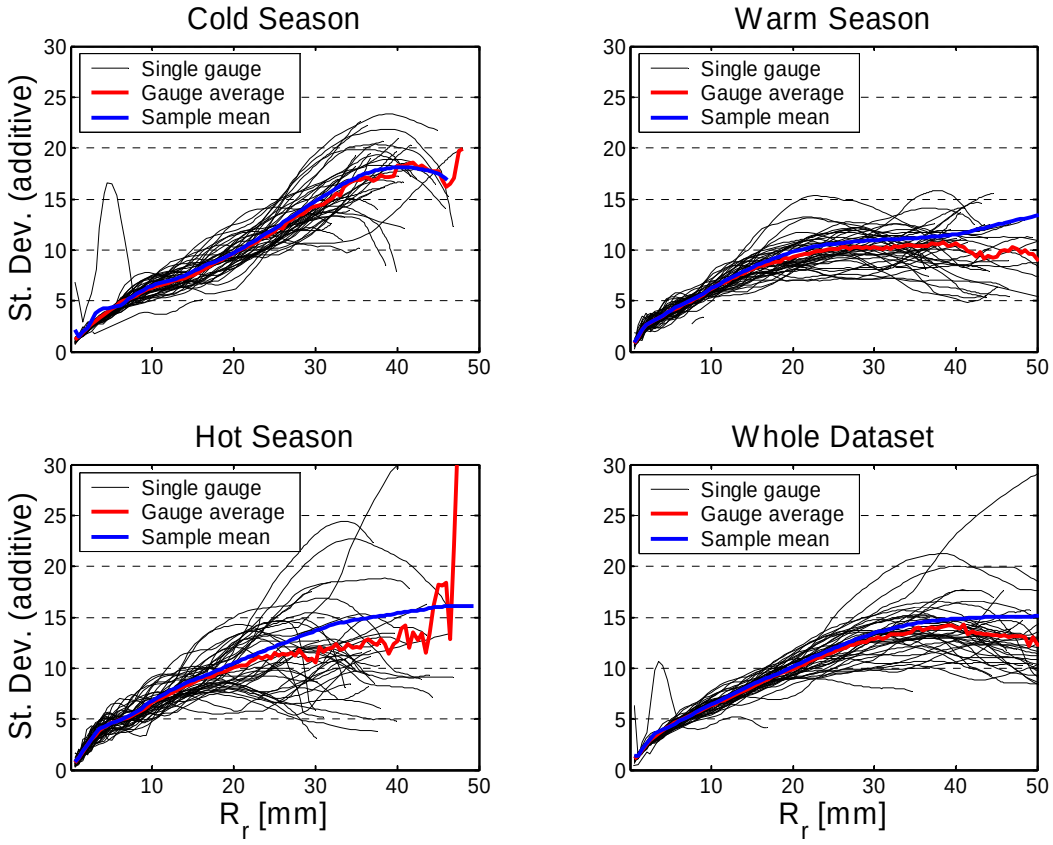

Fig. 25. Same as Figure 17, but for the 6-hour resolution.

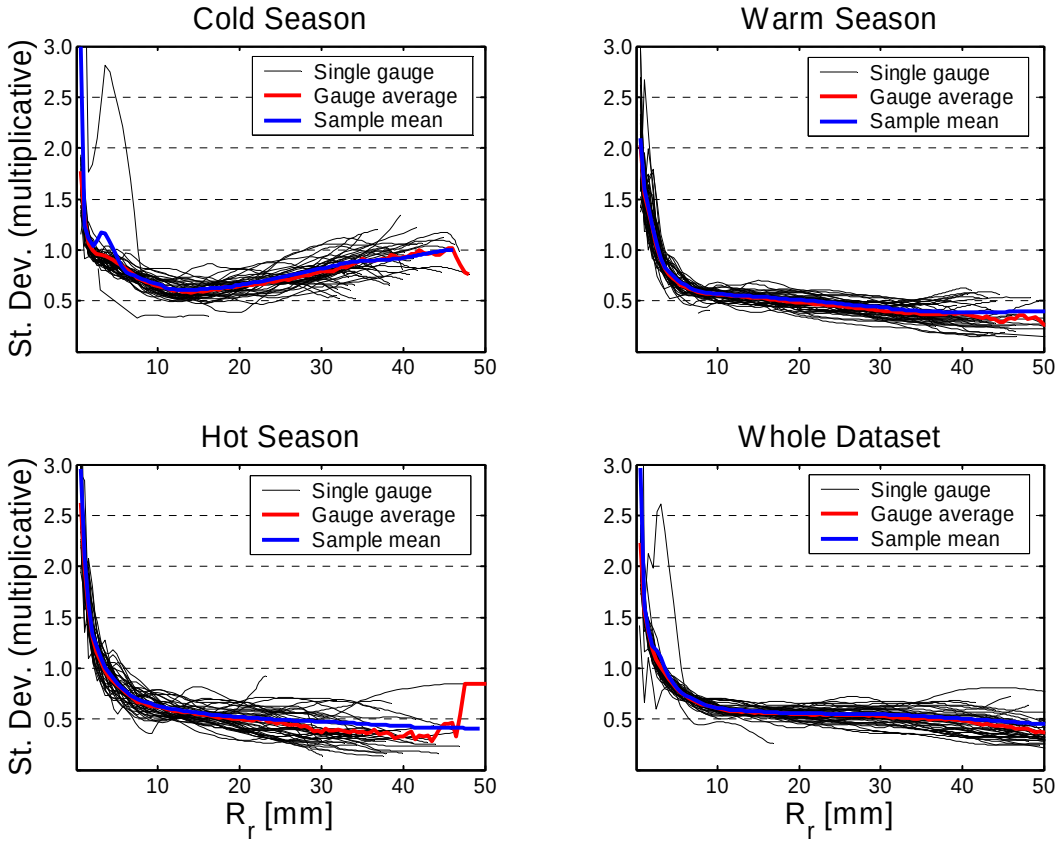

Fig. 26. Same as Figure 18, but for the 6-hour resolution.

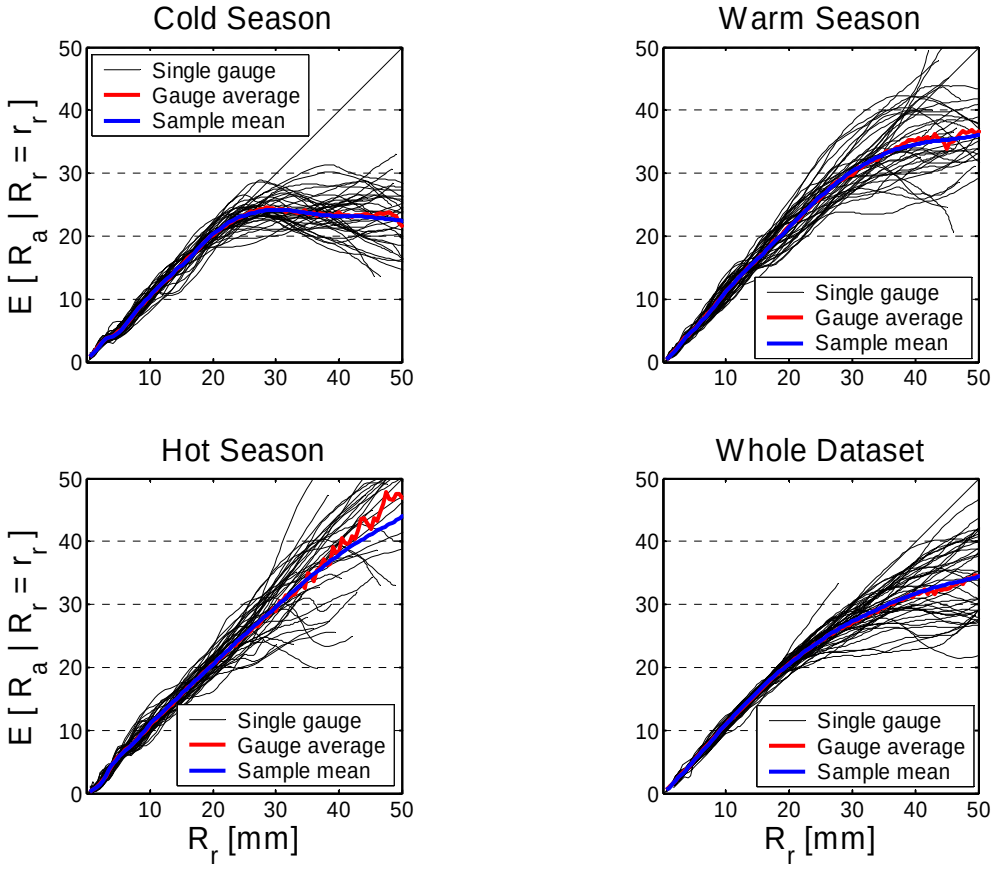

Fig. 27. Same as Figure 15, but for the 24-hour resolution.

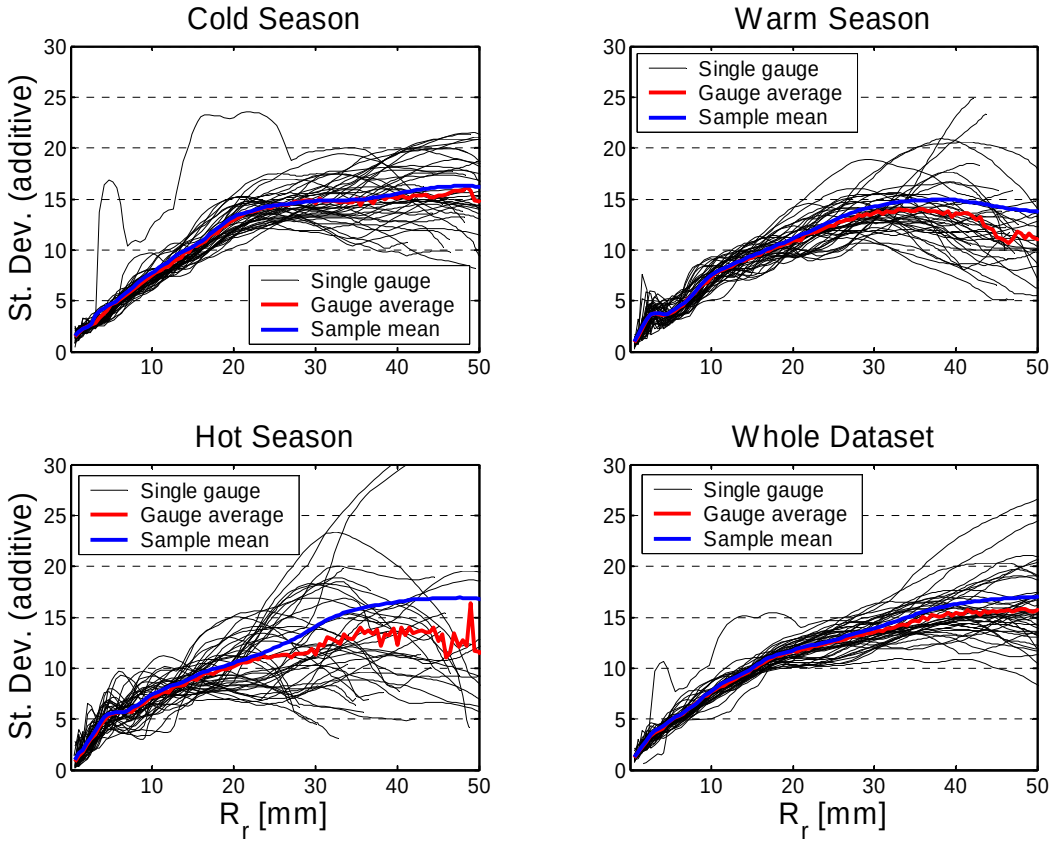

Fig. 28. Same as Figure 17, but for the 24-hour resolution.

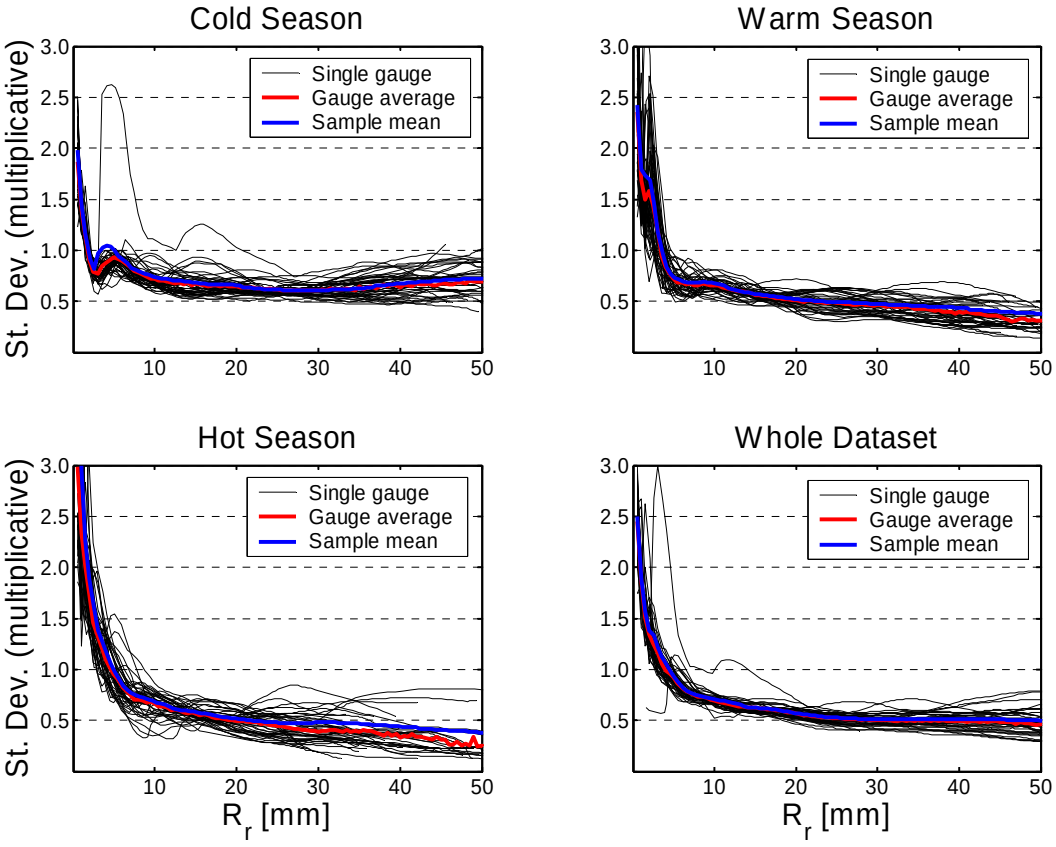

Fig. 29. Same as Figure 18, but for the 24-hour resolution.

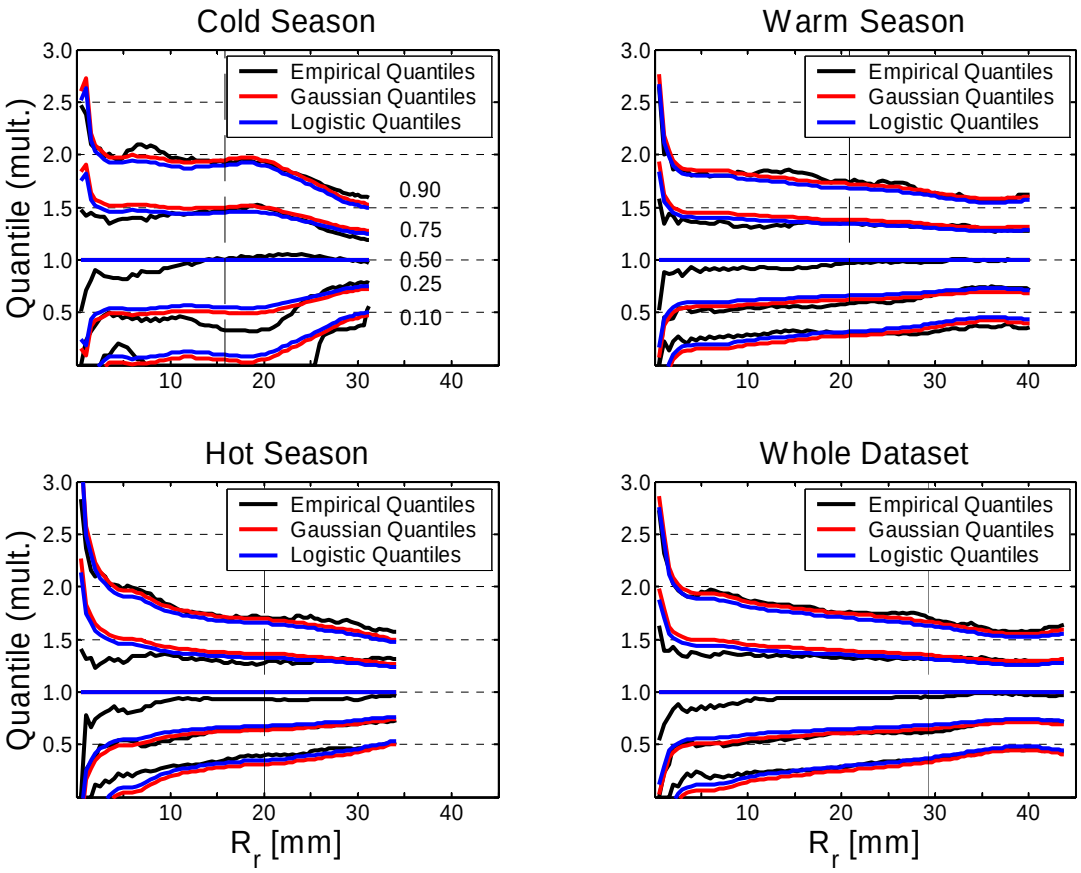

Fig. 30. Comparison of the empirical quantiles (0.1, 0.25, 0.5, 0.75, 0.9) with the corresponding quantiles from Gaussian and logistic distributions. For both of the theoretical distributions, the mean is equal to 1 and the standard deviation is the standard deviation of the random component in the multiplicative form. The segments on the left of the dashed vertical line are computed with a weighted sample size larger or equal to 1000, while the segments on the right with a weighted sample size between 1000 and 100. The temporal resolution is 1 hour.

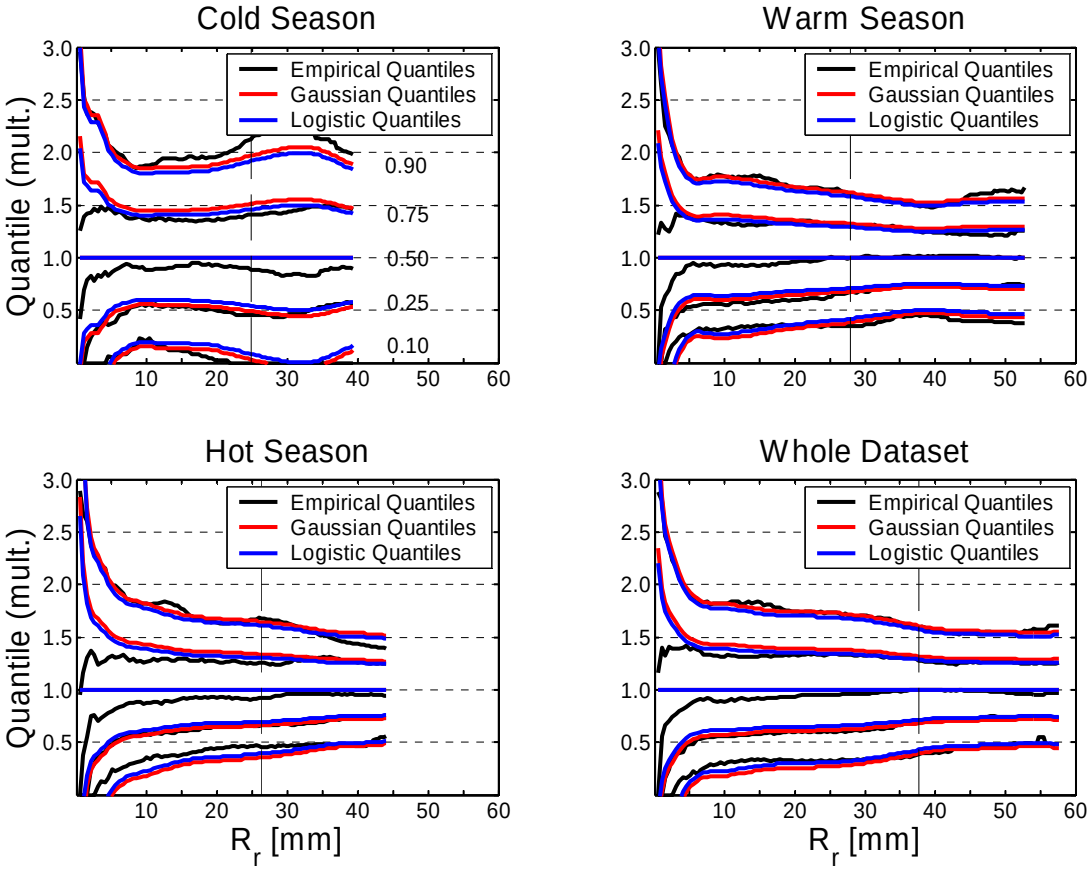

Fig. 31. Same as Figure 30 (previous page) but for the 3-hour temporal resolution.

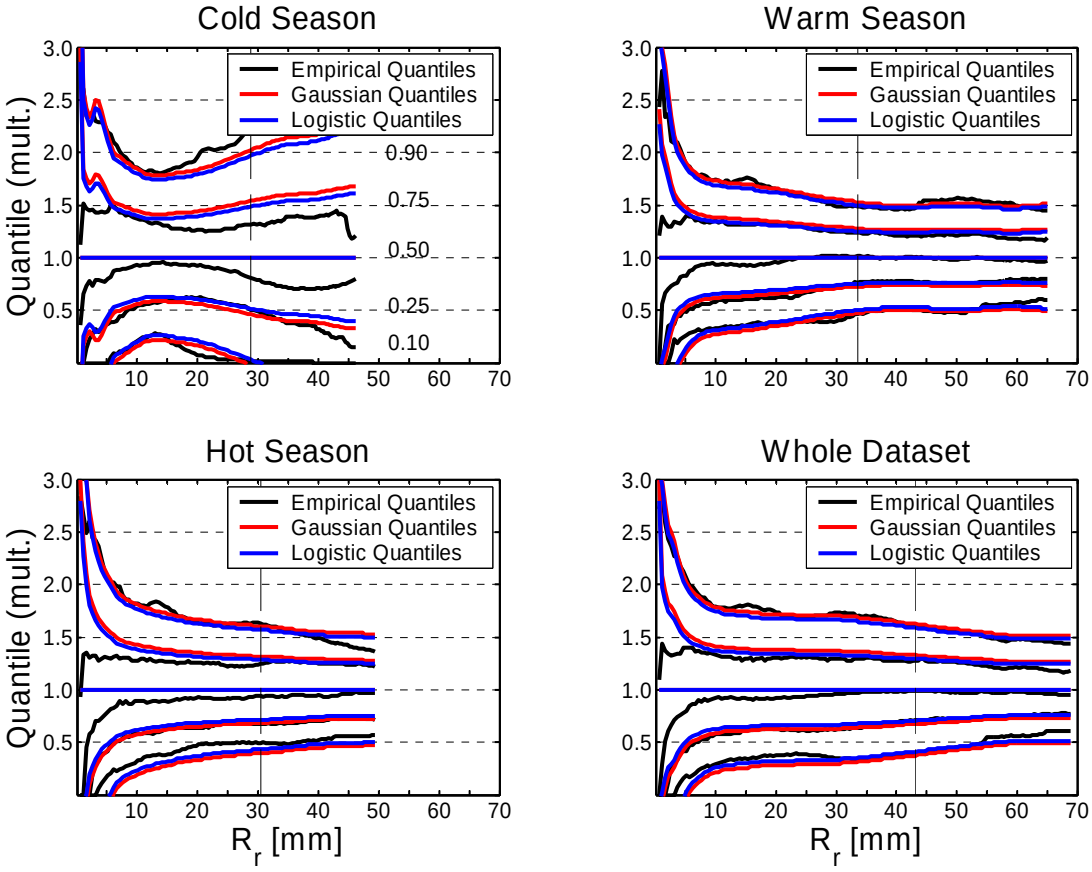

Fig. 32. Same as Figure 30 but for the 6-hour temporal resolution.

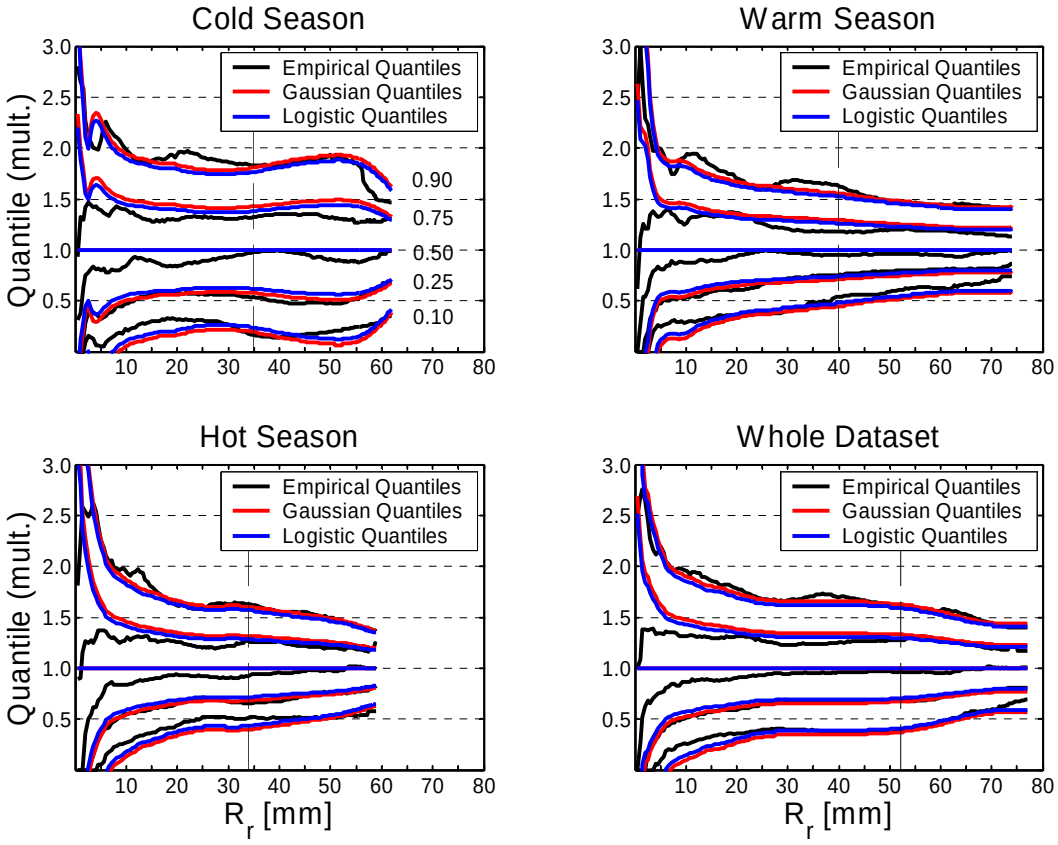

Fig. 33. Same as Figure 30 but for the 24-hour temporal resolution.

C.1.4. Error Dependence Analyses

C.1.4.1. *Temporal Correlation*

At present, the temporal correlation of the errors has not yet been characterized. Only very few studies have tried to account for it (e.g., Nijssen and Lettenmaier 2004; Hossain et al. 2004).

In Figure 34, we have plotted the temporal correlation of the random component of the error model in the multiplicative form for the hourly time resolution. It is possible to notice a quick drop up to around one hour and then a subsequent slower decrease. We think that this feature can be explained by the fact that the DPA product is a running 1-h rainfall accumulation and therefore, the information up to one-hour lag is not completely independent. It is also possible to notice a stronger correlation for the cold season compared to the other two.

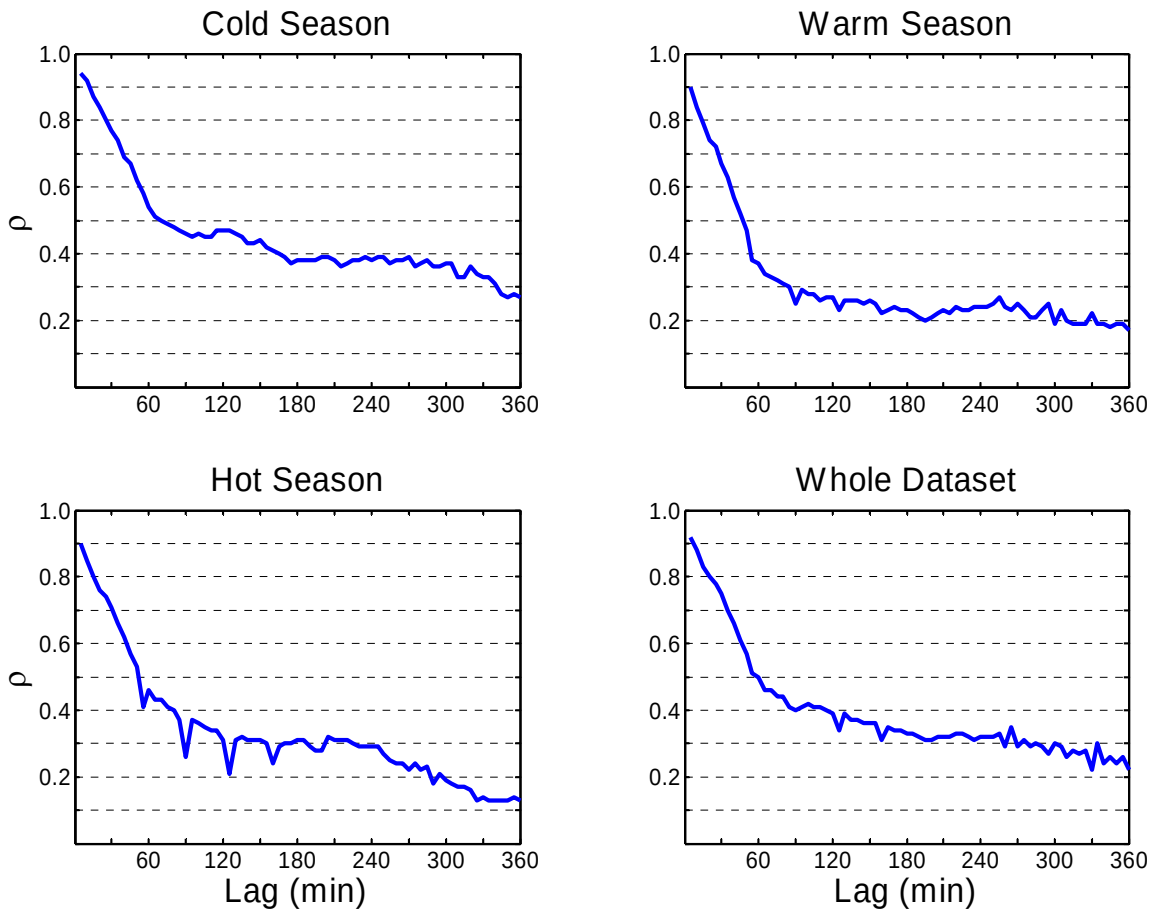

Fig. 34. Temporal correlation of the random component in the multiplicative form for the three seasons and the whole dataset.

C.1.4.2. *Spatial Correlation*

As for the temporal correlation, our current knowledge about the spatial correlation of the errors is extremely limited. Some studies have compared the possible effects in case of spatial correlation and uncorrelation, showing how the outcomes could be sensibly different (e.g., Nijssen and Lettenmaier 2004; Villarini et al. 2005).

In our study, we have found that the random component of the error in the multiplicative form is correlated in space (Figure 35). Compared to the spatial correlation estimated from the rain gauge data (Figure 11), the scatter is larger and the correlation is lower. However, some features, such as the series of points out of pattern in the cold season are the same.

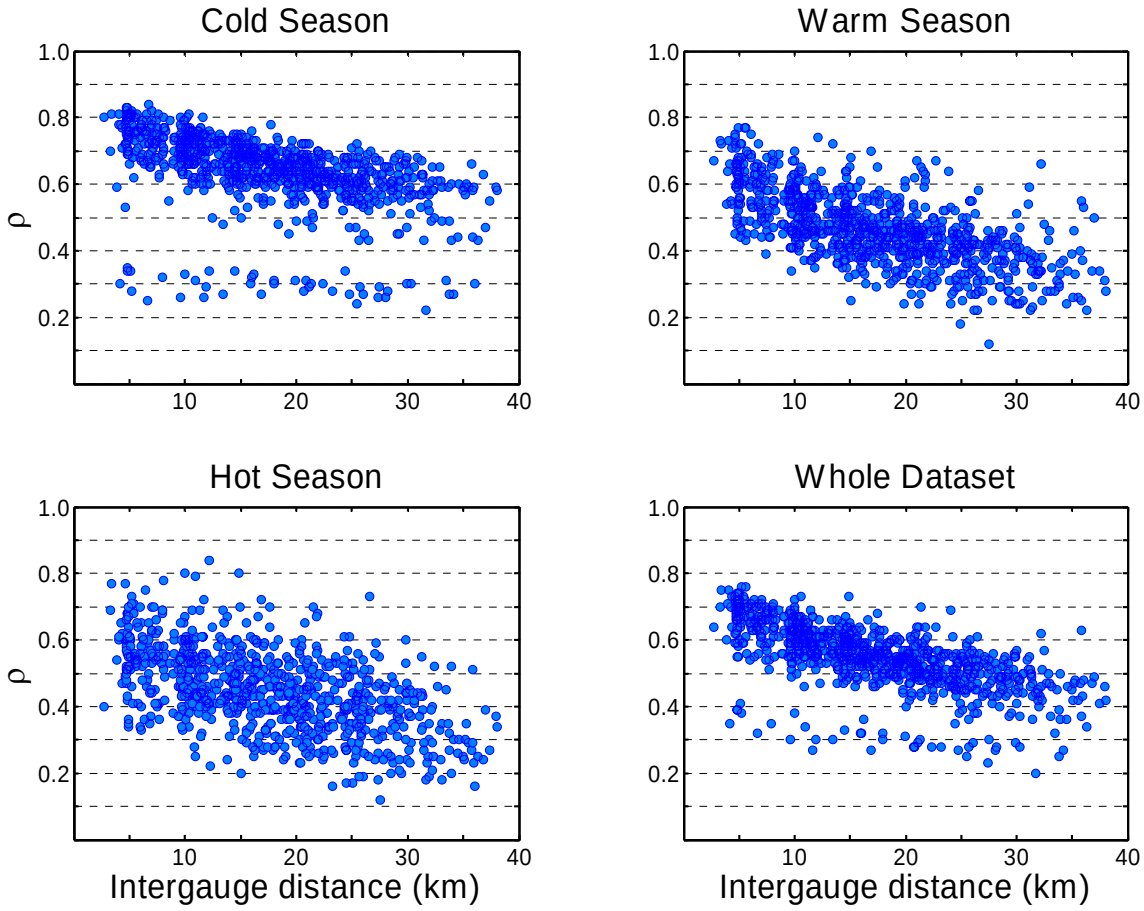

Fig. 35. Spatial correlation of the random component in the multiplicative form for the three seasons and the whole dataset.

D. ERROR MODELING

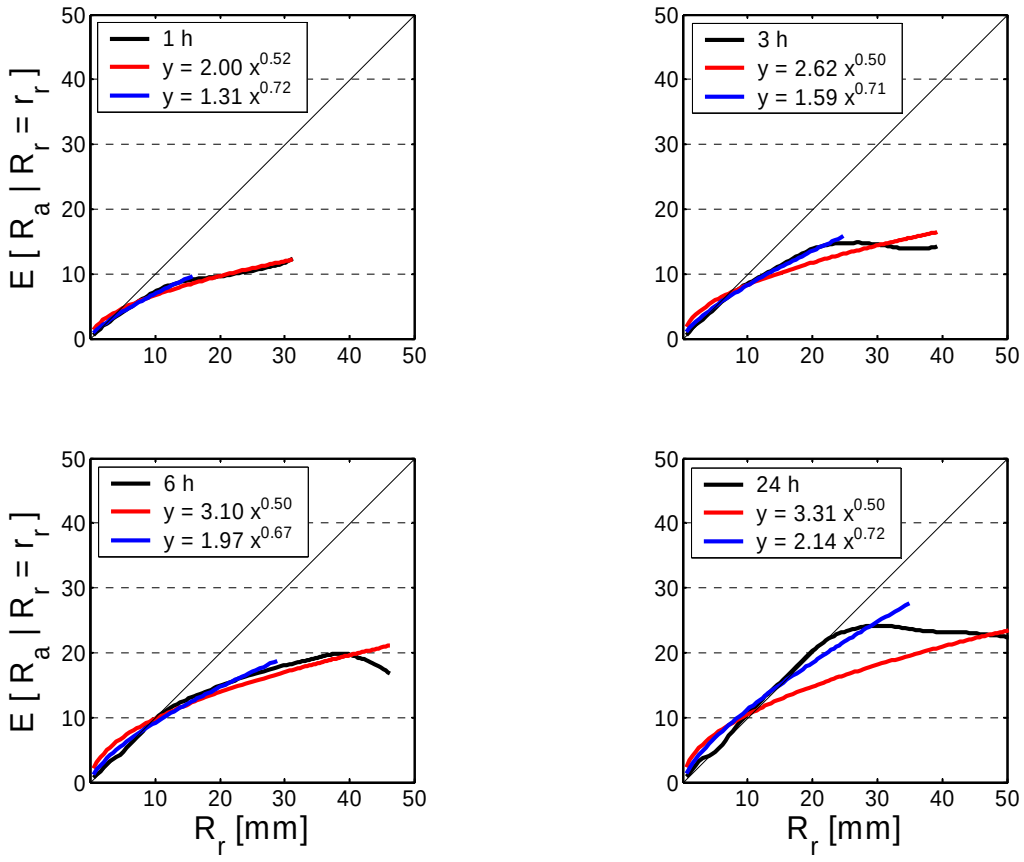

Fig. 36. Modeling of the rain gauge averages for the cold season, for the four temporal resolutions. The black lines corresponds to the empirical result, the red and blue lines are obtained from fitting the data with a power law up to a weighted sample size of 100 and 1000 respectively.

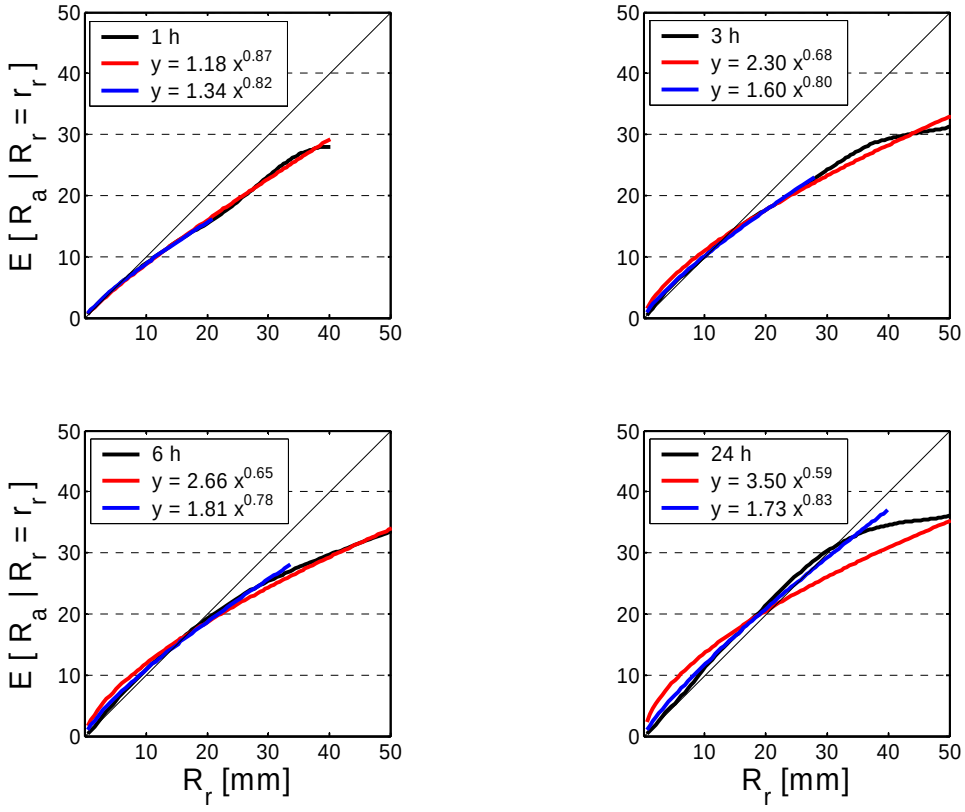

Fig. 37. Same as Figure 36 (in the previous page) but for the warm season.

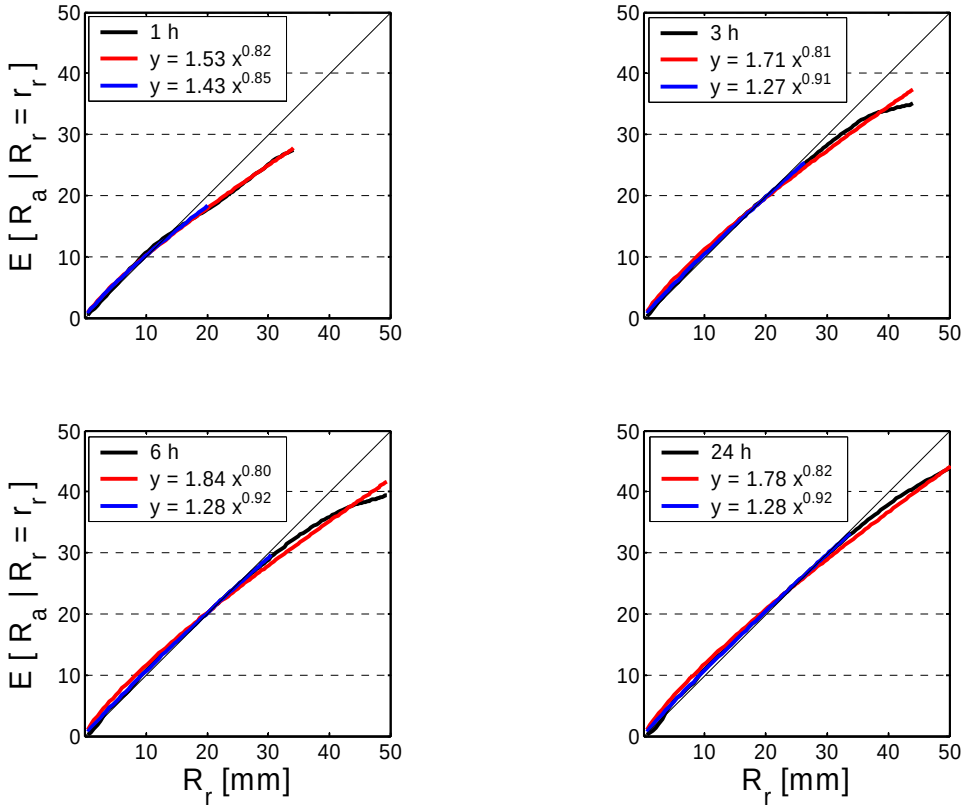

Fig. 38. Same as Figure 36 (two pages back) but for the hot season.

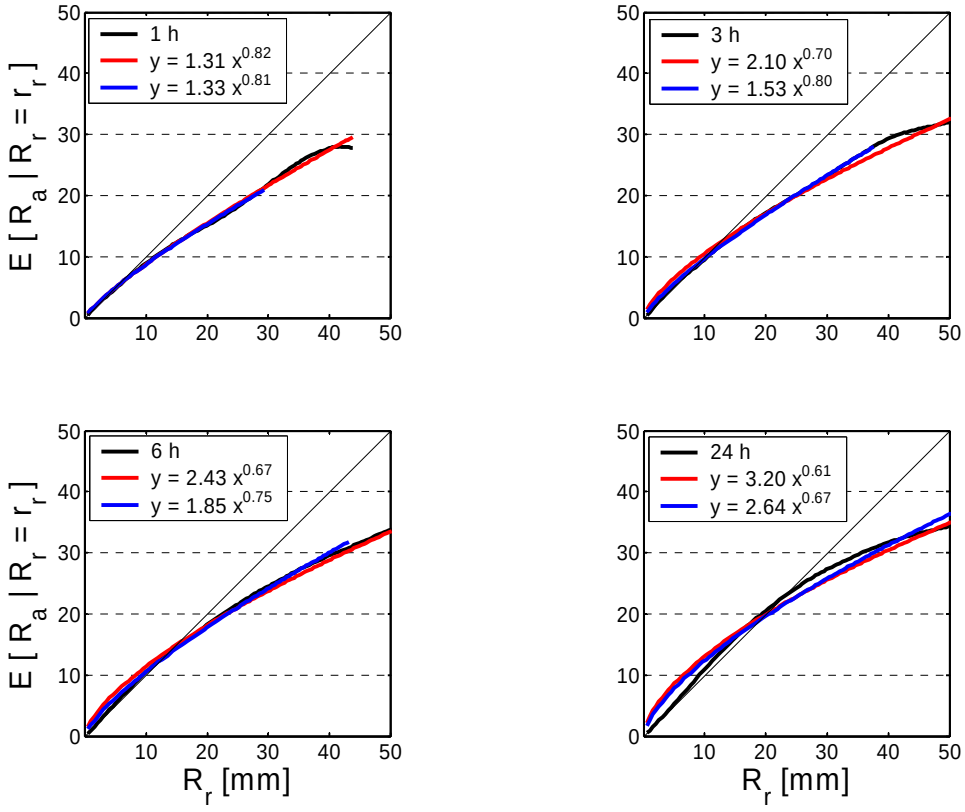

Fig. 39. Same as Figure 36 (three pages back) but for the whole dataset.

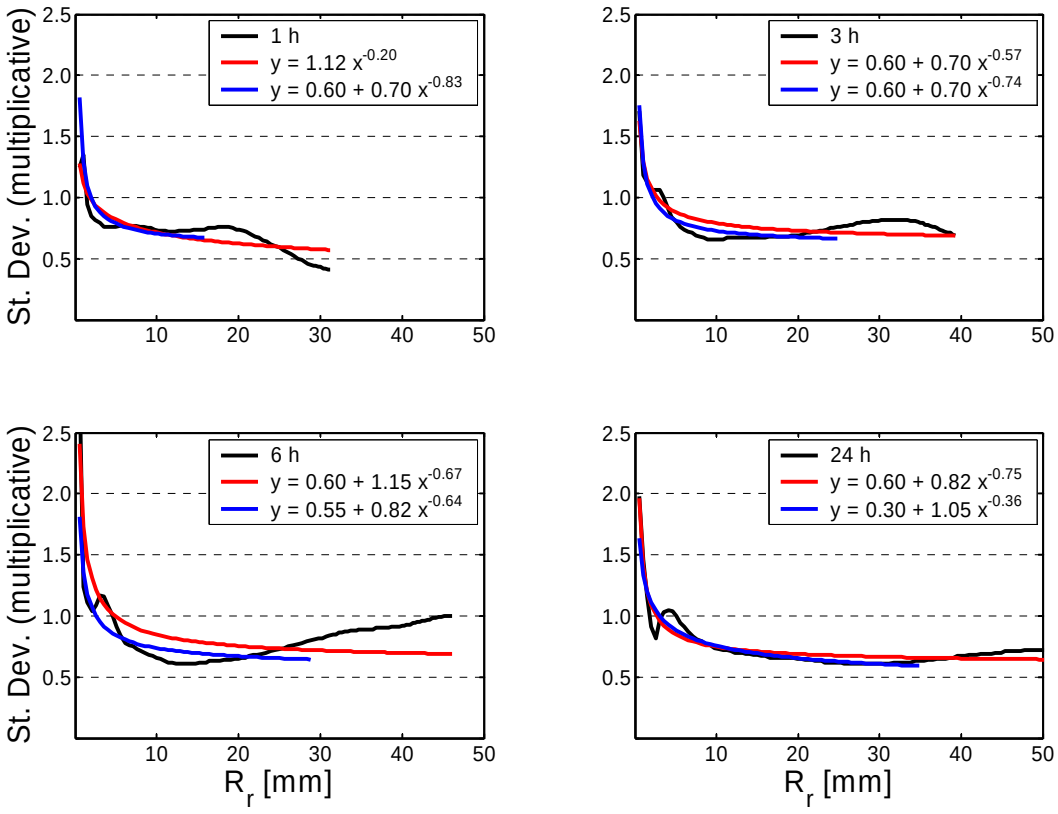

Fig. 40. Modeling of the standard deviation of the random component in the multiplicative form for the cold season, for the four temporal resolutions. The black lines corresponds to the empirical result, the red and blue lines are obtained from fitting the data with a power law up to a weighted sample size of 100 and 1000 respectively.

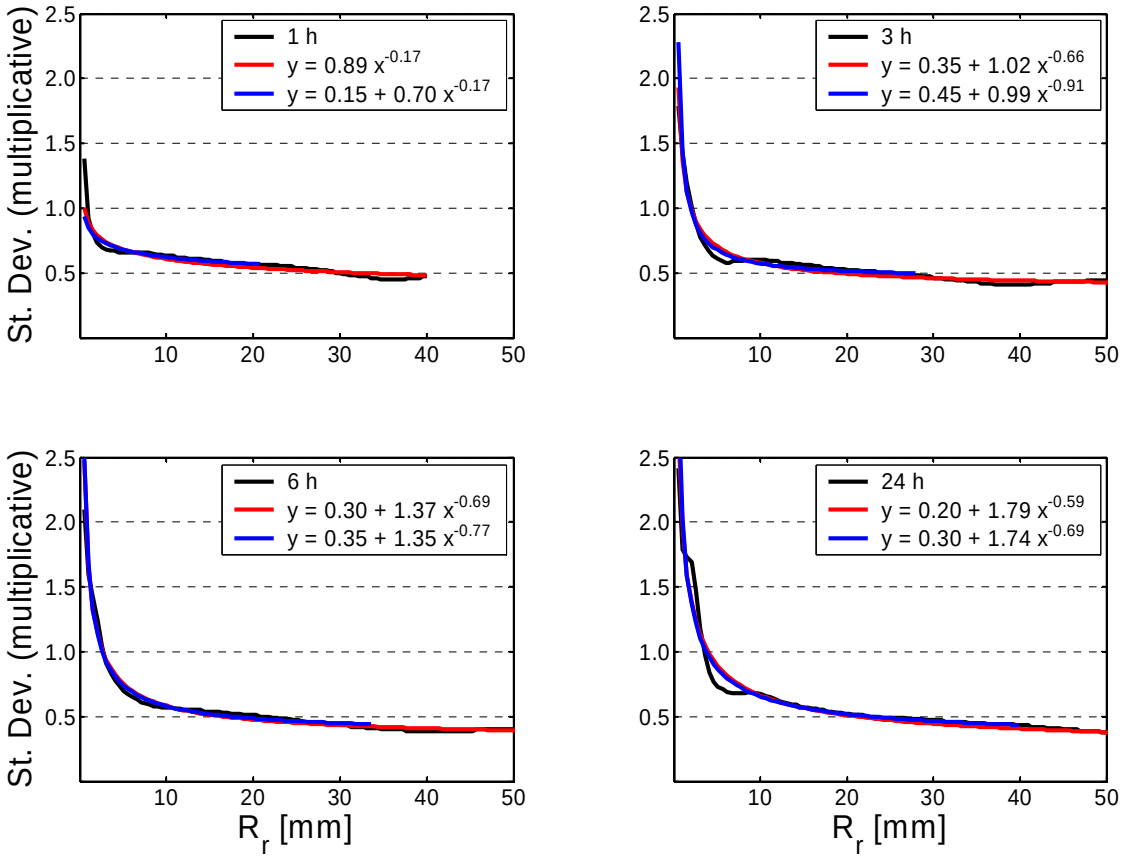

Fig. 41. Same as Figure 40 (in the previous page) but for the warm season.

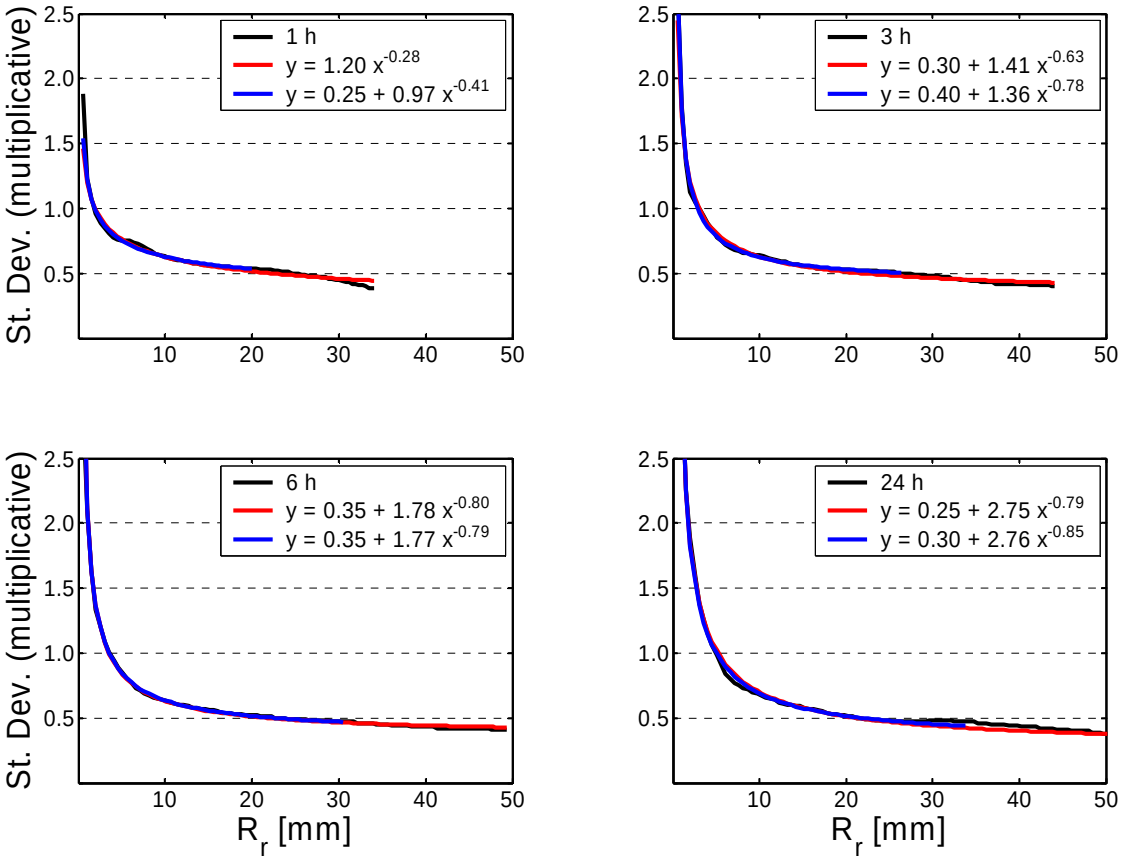

Fig. 42. Same as Figure 40 (two pages back) but for the hot season.

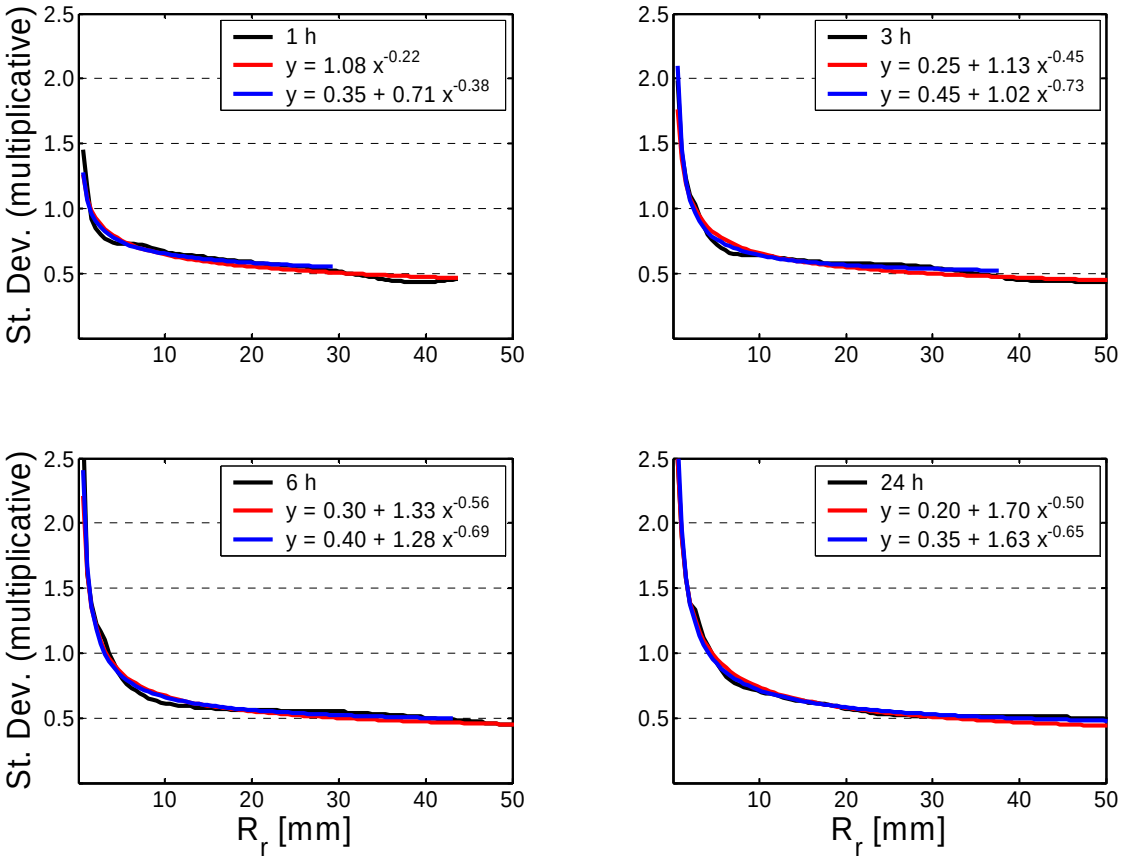

Fig. 43. Same as Figure 40 (three pages back) but for the whole dataset.

Bibliography

Austin, P.M., Relation between measured radar reflectivity and surface rainfall. *Monthly Weather Review*, 115, 1053-1070, 1987.

Brock, F.V., K.C. Crawford, R.L. Elliott, G.W. Cuperus, S.J. Stadler, H.L. Johnson and M.D. Eilts, The Oklahoma Mesonet: A technical overview, *Journal of Atmospheric and Oceanic Technology* 12(1), 5-19, 1995.

Carpenter, T.M., J.A. Sperfslage, K.P. Georgakakos, T. Sweeney and D.L. Fread, National threshold runoff estimation utilizing GIS in support of operational flash flood warning systems, *Journal of Hydrology*, 224, 21–44, 1999.

Carpenter, T.M., K.P. Georgakakos and J.A. Sperfslage, On the parametric and NEXRAD-radar sensitivities of a distributed hydrologic model suitable for operational use, *Journal of Hydrology*, 253(1-4), 169-193, 2001.

Ciach, G.J., and W.F. Krajewski, Analysis and modeling of spatial correlation structure in small-scale rainfall in central Oklahoma, submitted to *Advances in Water Resources*, 2005.

Ciach, G.J., E. Habib and W.F. Krajewski, Zero-covariance hypothesis in the Error Variance Separation method of radar rainfall verification, *Advances in Water Resources*, 26(5), 673-680, 2003.

Ciach, G.J., Local random errors in tipping-bucket raingauge measurements, *Journal of Atmospheric and Oceanic Technology*, 20, 752-759, 2003.

Ciach, G.J., M.L. Morrissey, and W.F. Krajewski, Conditional bias in radar rainfall estimation. *Journal of Applied Meteorology*, 39, 1941-1946, 2000.

Ciach, G.J., W.F. Krajewski, E.N. Anagnostou, M.L. Baeck, J.A. Smith, J.R. McCollum, and A. Kruger, Radar rainfall estimation for ground validation studies of the Tropical Rainfall Measuring Mission. *Journal of Applied Meteorology*, 36, 735-747, 1997.

Fread, D.L., R.C. Shedd, G.F. Smith, R. Farnsworth, C. Hoffeditz, L.A. Wenzel, S.M. Wiele, J.A. Smith, and G.N. Day, Modernization in the National Weather Service River and Flood Program. *Weather and Forecasting*, 10(3), 1995.

Fulton, R.A., J.P. Breidenbach, D-J. Seo, D.A. Miller, and T. O'Bannon, The WSR-88D Rainfall Algorithm. *Weather and Forecasting*, 13, 377-395, 1998.

Georgakakos, K.P., Guetter, A. K. and J. A. Sperfslage, Estimation of flash flood potential for large areas. Destructive Water: Water-Caused Natural Disasters, their Abatement and Control. G.H. Leavesley, H.F. Lins, F. Nobilis, R.S. Parker, V.R. Schneider, and F.H.M.van de Von (eds.), *IAHS Publ. No. **239**, IAHS Press, Wallingford*, UK, 87-93, 1997.

Habib, E., Ciach, G.J., and W.F. Krajewski, A method for filtering out raingauge representativeness errors from the verification distributions of radar and raingauge rainfall. *Advances in Water Resources*, 2004, (in press).

Hardle, W., *Applied Nonparametric Regression*. Cambridge University Press, 333 pp., 1990.

Hossain, F., E.N. Anagnostou and T. Dinku, Sensitivity analyses of satellite rainfall retrieval and sampling error on flood prediction uncertainties, *IEEE Transactions on Geoscience and Remote Sensing*, 42(1), 130-139, 2004.

Journel, A.G., and C.H.J. Huijbregts, *Mining Geostatistics*. Academic Press, 598 pp., 1978.

Krajewski, W.F. and G.J. Ciach, Towards probabilistic quantitative precipitation WSR-88D algorithms: Preliminary studies and problem formulation, *Final Report for the NWS Office of Hydrologic Development*, Silver Spring, Maryland, pp. 59, 2003.

Krajewski, W.F. and J.A. Smith, Radar hydrology: Rainfall estimation, *Advances in Water Resources*, 25, 1387–1394, 2002.

Krajewski, W.F. and K.P. Georgakakos, Synthesis of radar-rainfall data, *Water Resources Research*, 21(5), 764-768, 1985.

Krajewski, W.F., G.J. Ciach and E. Habib, An analysis of small-scale rainfall variability in different climatological regimes, *Hydrologic Sciences Journal*, 48(2), 151-162, 2003.

Krzysztofowicz, R., The case for probabilistic forecasting in hydrology, *Journal of Hydrology*, 249, 2-9, 2001.

Morrissey, M.L., 1991: Using sparse raingages to test satellite-based rainfall algorithms. *J. Geophys. Res.*, 96, 18561-18571.

Nijssen, B., and D.P. Lettenmaier, Effect of precipitation sampling error on simulated hydrological fluxes and states: anticipating the Global Precipitation Measurement satellites, *Journal of Geophysical Research*, 109, D02103, doi:10.1029/2003JD003497, 2004.

Petersen-Øverleir, A., Misspecification of extreme rainfall population and frequency inference due to measurement bias and variability, *Atmospheric Research*, 75, 283-300, 2005.

Reed, S., D. Johnson and T. Sweeney, Application and national geographic information system database to support two-year flood and threshold runoff estimates, *Journal of Hydrologic Engineering*, **7**(3), 209-219, 2002.

Reed, S.M. and D.R. Maidment, Coordinate transformation for using NEXRAD data in GIS-based hydrologic modeling, *Journal of Hydraulic Engineering*, 174-182, 1999.

Simonoff, J.S., *Smoothing Methods in Statistics*. Springer-Verlag, 338 pp., 1996.

Vignal, B. and W.F. Krajewski, Large sample evaluation of two methods to correct range-dependent error for WSR-88D rainfall estimates, *Journal of Hydrometeorology*, 2(5), 490-504, 2001.

Villarini, G., G.J. Ciach, W.K. Krajewski, K. Nordstrom, and V.J. Gupta, Impact of systematic and random errors in scaling properties of radar rainfall, to be submitted to *Journal of Geophysical Research*, 2005.